The Effects of Rain on Topex Radar Altimeter Data

G. D. QUARTLY,* T. H. GUYMER, AND M. A. SROKOSZ*

Southampton Oceanography Centre, Empress Dock, Southampton, Hants, United Kingdom

(Manuscript received 22 June 1995, in final form 24 April 1996)

ABSTRACT

Rain has long been categorized as a contaminant of altimeter data, but little has been done previously to ascertain the magnitude and frequency of its effect or its geographical distribution. Proceeding from recent analysis of *ERS-1* data, and the insight gained, this paper addresses all these issues, highlighting the particular advantages of Topex's dual-frequency capability.

The primary effect of rain is on the observed backscatter values σ^0 through attenuation of the radar signal. An empirical relationship is derived linking the observed σ^0 values at C band and K_u band. Through a series of case studies and global analyses, prominent departures from this relationship are shown to be caused by regions of significant precipitation. As it is predominantly the K_u-band returns that are affected, C-band σ^0's are likely to be of great use for the determination of wind speeds in regions or events of intense rain. The different attenuation rates give dual-frequency altimetry the potential to yield information on rain distribution and intensity that complement that achievable by infrared sensors alone.

1. Introduction

As altimeter measurements over the oceans become increasingly accurate (see, e.g., Marth et al. 1993) the need for better corrections and for better flagging of incorrect data becomes paramount. One source of error in altimeter data is that due to the presence of rain in the atmosphere, which affects the altimeter return signal from the sea surface. In a series of earlier papers (Srokosz and Guymer 1988; Guymer and Quartly 1993; Quartly et al. 1994; Guymer et al. 1995, hereafter GQS) we have studied the effects of rain on the K_u-band altimeters flown on Seasat and *ERS-1*. (Note that Geosat's severe mispointing problems make it difficult to analyse the effects of rain on its data.) The purpose of this paper is to extend those studies to the K_u- and C-band data from the Topex altimeter.

As a result of the studies with Seasat and *ERS-1* data, what is our state of knowledge about rain effects on altimeter returns from the sea surface? The following summarizes the results obtained to date.

(a) The primary effect of rain is to attenuate the signal, thus reducing the backscattered power σ^0. As the wind speed U_{10} is estimated from σ^0, this can lead to significant errors in U_{10}.

(b) At higher rain rates (>20 mm h^{-1}) the effect of rain can distort the shape of the return waveform and so affect the estimates of the altimetric height h and the significant wave height H_s. In extreme cases the waveform shape is so distorted that the altimeter tracker suffers "loss of lock" and ceases to track the sea surface. This results in the total loss of data from the altimeter until the tracker reacquires lock on the sea surface.

(c) A small number of cases of enhanced backscatter in the presence of rain were found. A possible explanation for these observations is the damping of small-scale waves by the rain and the consequent reduction of the mean square wave slope s^2, leading to an increase σ^0 (as they are inversely related; Barrick 1974). However, other explanations may exist [a recent paper by Atlas (1994) discusses various rain effects on SAR data that may, or may not, be relevant to the altimeter case].

(d) For *ERS-1* it may be possible to flag occurrences of rain-affected data by using criteria based on a combination of the standard deviation of the 1-s altimetric height estimates and the predicted liquid water attenuation estimated from the onboard radiometer (the predicted attenuation was found to be too small, so it could not be used to correct the data but could be used to flag it; see GQS).

Here the studies with Seasat and *ERS-1* are extended to consider rain effects on Topex altimeter data. We have confined ourselves exclusively to the Topex altimeter for two reasons. 1) The Poseidon altimeter on the same satellite platform is only in operation 10% of the time, making it harder to obtain meaningful statistics

* Additional affiliation: Remote Sensing Applications Development Unit, Southampton, United Kingdom.

Corresponding author address: Dr. Graham D. Quartly, RSADU, Southampton Oceanography Centre, Empress Dock, Southampton SO14 3ZH, United Kingdom.

for it; and 2) we have already undertaken an investigation of the response of *ERS-1*'s K_u-band altimeter to rain cells (see GQS) and wish to concentrate here on the added insight obtained from Topex's two frequencies. Being a dual-frequency altimeter (K_u and C bands), and with a three-frequency passive microwave radiometer being flown on the same satellite (Marth et al. 1993), Topex presents a new and improved means of studying the effects of rain. First, the effect of rain depends on the radar frequency, being much less at C band than at K_u band (Farrow 1975; Walsh et al. 1984), so that it is possible to exploit the dual-frequency capability of Topex to gain new insight into this problem. Second, while *ERS-1* possessed a dual-frequency passive microwave radiometer that gave some indication of the presence of rain (Eymard et al. 1994), the three-frequency one on Topex gives improved information on the water content (whether vapour or liquid) of the troposphere and therefore should make it easier to confirm the presence or absence of rain.

The layout of this paper is as follows. In section 2 the differences between *ERS-1* and Topex instrumentation are discussed in more detail and the method adopted to study the problem is explained. Section 3 concentrates on the relationship between backscatter values observed at K_u and C bands; the first part details the present understanding of radar interaction with the sea and the results of attempts to derive such a relationship on theoretical grounds, while the second part describes the technique used to determine an empirical relationship pertinent to actual Topex data.

This relationship is crucial to the case studies discussed in section 4, which illustrate the range of effects observed in the backscatter data. In section 5, rain observations derived by altimetry are compared to those from the onboard microwave radiometer, while section 6 illustrates how altimetry may be used for studying rainfall patterns. Section 7 gives the conclusions of this study, indicating both the caution required in use of K_u-band altimetry and the improved analysis possible with the advent of dual-frequency altimetry.

2. Data source and method of analysis

Before describing the method adopted to study the problem (see section 2c), a brief review is given of the relevant instrumentation, comparing it to that on *ERS-1*. This is a necessary introduction to the approach adopted in this study, which varies somewhat from the earlier work on *ERS-1* (GQS).

a. Differences between Topex and ERS-1

As noted in the introduction, the two major differences between the *ERS-1* radar altimeter system and the Topex one are

- the dual-frequency K_u and C bands (13.6 and 5.3 GHz, respectively) capability of Topex (Marth et al. 1993), as opposed to the single-frequency K_u band (13.8 GHz) one on *ERS-1* (Francis et al. 1991); and
- the three-frequency (18.0, 21.0, and 37.0 GHz) Topex Microwave Radiometer (TMR) carried on the Topex/Poseidon platform for tropospheric corrections (Benada 1993; Callahan 1993), as opposed to the dual-frequency (23.8 and 36.5 GHz) radiometer on *ERS-1* (Eymard et al. 1994).

The primary reason for Topex being a dual-frequency altimeter is in order to correct for the propagation delay of radar pulses through the ionosphere, which varies with frequency (Callahan 1993). Water in both liquid and vapor forms causes a propagation delay too, but its effect varies little with radar frequency. However, through attenuation, cloud liquid water and rain are known to affect the *intensity* of a radar signal in a manner that does vary markedly with frequency (Farrow 1975; Walsh et al. 1984). We wish to explore the possibility of using this differential attenuation to eliminate the effects of rain in the data. To illustrate the importance of this effect, it is sufficient to note that for a rain cell 5 km in vertical extent and over a range of rain rates, the attenuation of the signal at C-band is an order of magnitude smaller than that at K_u band (Walsh et al. 1984). Therefore, particularly at low rain rates, the effect of rain on the C-band signal will be negligible so it may be possible to correct for rain effects in the K_u-band data.

The K_u-band (13.6 GHz) and C-band (5.3 GHz) altimeters share much of the transmit and receive hardware in common. The altimeter antenna is 1.5 m wide, resulting in a beamwidth of 1.1° at K_u band and 2.7° at C band (Callahan 1993). However, the altimeter operates in pulse-limited rather than beam-limited mode (see Chelton et al. 1989), with an effective pulse width of 3.125 ns for both channels, leading to a footprint only a few kilometers across. At K_u band, the pulse repetition frequency (PRF) is 4200 Hz, with radar returns averaged in groups of 228; for C band, the PRF is 1220 Hz, with 60 pulses averaged at a time. Prior to telemetry, these 20-Hz waveforms at both frequencies are further averaged to 10 Hz for K_u band (corresponding to 456 pulses) and 5 Hz for C band (240 pulses). [For comparison, the antenna size on *ERS-1* is 1.2 m, and its PRF is 1020 Hz (Francis et al. 1991), with 20-Hz waveforms (50 pulses averaged) being transmitted.] By matching these waveforms to that expected for an oceanlike surface (Chelton et al. 1989), various geophysical variables may be derived for each frequency. These are then averaged together to give 1-Hz values for significant wave height H_s, backscatter σ^0, range to sea surface, and waveform-derived attitude. The first two of these are provided as separate values for each frequency: range is a single term, calculated from both K_u- and C-band returns, using their difference to estimate the ionospheric correction; and attitude is derived solely from the K_u-band waveforms.

b. *Topex Microwave Radiometer and derived variables*

One of the auxiliary instruments on the Topex/Poseidon platform is the Topex Microwave Radiometer (TMR), which observes the brightness temperatures T_b of the near-nadir region at three different frequencies—18, 21, and 37 GHz. These values are all smoothed to 42 km, which is the footprint corresponding to the beamwidth of the lowest frequency. (The footprint size for *ERS-1*'s ATSR/M is approximately one-half of that of the TMR.) Over ocean, the brightness temperatures are typically in the region of 140–180 K; these values are much lower than the sea surface temperature because of the low emissivity of water at these frequencies. Clouds on the other hand have a high emissivity, so temperatures greater than 250 K may be recorded. An empirical fit of brightness temperature data to 8000 radiosonde measurements (Callahan 1996, personal communication) led to a simple polynomial formula for the liquid water path (LWP). This relationship, recommended for use with the GDR data, is given by

$$L = -2.28036 - 0.012241T_b\,(18\text{ GHz}) - 0.005128T_b\,(21\text{ GHz}) + 0.028964T_b\,(37\text{ GHz}) \quad (1a)$$

$$\text{LWP} = \begin{cases} L, & L \leq 0.6\text{ mm} \\ L + 0.43(L-0.6) + 0.3(L-0.6)^2, & L > 0.6\text{ mm}, \end{cases} \quad (1b)$$

where L and LWP are in millimeters of water, and the T_b's are in kelvins. [A liquid water path of 1 mm is equivalent to a liquid water content (mass of water column per unit area) of 1 kg m^{-2}.] As this is an approximation, small negative values may result; these are set to zero. Each data record also contains a rain flag, which is set if the LWP exceeds a threshold (1.0 mm) or if T_b (37 GHz) is greater than 250 K. A rain flag was provided with the *ERS-1* altimeter data, based on the ATSR/M brightness temperatures, but the algorithm implemented was not correct (Stum 1994, personal communication). As part of this study, the efficacy, or otherwise, of the Topex rain flag is investigated.

An estimated level of attenuation is also derived from the TMR output. The two-way correction $\delta\sigma^0$ is a function of the derived levels of water in its liquid and gaseous form and is expressed (Callahan 1994, personal communication) in terms of LWP and δh_v (the height correction in millimeters due to water vapor) as

$$\delta\sigma^0 = 2 \times 10 \log_{10} e(0.01362 + 0.000055|\delta h_v| + 0.032896\text{ LWP}). \quad (2)$$

Since LWP is rarely more than 1 mm, while δh_v can be around 400 mm in the Tropics, their contributions to $\delta\sigma^0$ are of similar magnitude. The $\delta\sigma^0$ correction serves to raise the original uncorrected σ^0 values by between 0.12 and 1.0 dB; its mean is 0.22 dB, with a standard deviation (sd) of 0.07 dB, and the default (clear sky) value is 0.12 dB. In situations of extreme rain, the $\delta\sigma^0$ values in the GDR revert to their default value, that is, no attempt is made to give realistic estimates of the attenuation. (In the case of *ERS-1* traversing strong rain events, it was shown by GQS that its supplied attenuation correction underestimated the reduction in observed backscatter by typically a factor of 3.5.)

c. *Method of analysis*

The investigations detailed in sections 3 and 5 are based on large sets of global data, treating each data record separately. However, in order to explore the spatial structure of the fields affected by atmospheric events, it is necessary to examine a few particular cases. The method of selection used made no use of the dual-frequency altimetry nor of the data from the TMR. Instead, we located cases where the K_u-band σ^0 values changed sharply, assuming that attenuation by rain would be a much more likely cause than some real variation in the wind field.

This is deliberately identical to the approach used for case selection on our earlier studies with *ERS-1* (GQS). In that work, only K_u-band σ^0 data below 12 dB were used (in order to avoid situations with calm seas or sea ice, which both yield high σ^0 values), with events selected if the smoothed σ^0 values contained a "jump" in σ^0 of 2 dB or more in eight records or less. To achieve compatibility for Topex, the threshold was increased to 12.7 dB to allow for Topex's higher σ^0 values (Callahan et al. 1994b), and the search conducted over intervals of up to nine records to allow for Topex's slightly slower ground track velocity due to its higher orbit. With these adaptations, the number of events found in a 2-month period (see Fig. 11) was 101; a series of analyses with *ERS-1* yielded between 42 and 91 events per month, with an average of 61. Thus, the above changes appear to make the algorithm consistent between the different satellite datasets.

Clearly such a method does not prove perfect at detecting cases of rain; light to moderate rainfall events are not detected since the attenuation is not great enough, while some storm systems can cause such a sharp change by wind alone. These two different causes can often be distinguished by examining the detailed structure of the σ^0 profile at K_u band; the additional information from the TMR helps clarify the interpretations. Greater insight can be obtained by noting the difference in σ^0 structure at K_u and C bands. For this, one needs to know the relationship between the backscatters at the two frequencies in the absence of rain. This is the subject of the following section, in which a mean relationship between the two backscatter terms is obtained and subsequently used in the analyses throughout the rest of this paper.

3. Relating the K_u- and C-band backscatter

In section 3b an empirical relationship between the backscattered power σ^0 at K_u and C bands will be obtained from the Topex data and used to study the effects of rain. Ideally it would be better to obtain a theoretical relationship between the values at the two frequencies rather than rely on an empirically derived one. First, in section 3a we discuss whether it is possible to obtain such a relationship theoretically.

a. Theoretical background

Understanding of radar altimeter backscatter from the sea surface is fundamentally based on a geometrical optics theory that assumes that the backscattered power is independent of the radar frequency (Stewart 1985; Brown 1978). Under these assumptions Barrick (1974) has shown that the backscattered power σ^0 is given by

$$\sigma^0 = \frac{|R(0)|^2}{s^2}, \tag{3}$$

where $R(0)$ is the Fresnel reflection coefficient at zero degrees incidence and s^2 is the mean square wave slope. The only direct influence of radar frequency in (3) is the value of the Fresnel reflection coefficient $R(0)$, which is frequency dependent [since it depends on the dielectric constant of seawater (Klein and Swift 1977)]. However, there is an indirect influence through the value of s^2 in the following way. The value of s^2 is critically dependent on how it is evaluated in terms of the high wavenumber cutoff of the wave spectrum (Jackson et al. 1992). Now for Topex the radar wavelength at K_u band is 2.2 cm, while at C band it is 5.7 cm. High wavenumber waves exist on the sea surface with wavelengths in the range of the radar wavelengths, which contribute to s^2, and the geometrical optics theory does not describe the scattering effects occurring at these scales [it effectively treats the surface as smooth at small scales (Brown 1978)]. So the question is, what is the correct value to be used for s^2 in (3) at the different radar frequencies? Or is an improved theory necessary to account for scattering effects on scales at the sea surface that are comparable to the radar wavelength?

Brown (1978; see also Jackson et al. 1992) approached this problem by splitting the surface into a large- and a small-scale component relative to the radar wavelength, for which he assumed that geometrical optics and small-scale diffraction theory were applicable, respectively. The division occurs at a wavenumber that depends on the spectrum of surface and on the radar wavenumber. Following this lead, a number of models of the wave spectrum were used to compute s^2, with a variety of radar wavelength-dependent cutoffs, to obtain σ^0 at C and K_u bands. It was found that it was only possible to explain a difference of 1–2 dB between the C- and K_u-band values of σ^0 (C-band values are greater than K_u-band ones for a given wind speed). Empirically (see section 3b) it was found that the differences were of the order of 3–4 dB.

It might be considered that the theory used here is too simple to correctly represent the physics of the problem, but the more complex scattering simulations of Rodriguez et al. (1992) give similar differences between C- and K_u-band values of σ^0 (see their Fig. 7) for wind speeds of 5–12 m s^{-1}. Although Rodriguez et al. (1992) used more sophisticated models of both the radar scattering and the wave field than used here, their simulations were restricted (by computer power) to a sea surface that varied in one horizontal dimension only. It is unclear whether, using their approach, even with a fully two-dimensional sea surface model, it would be possible to explain the C-band–K_u-band differences for two reasons. First, as noted by Rodriguez et al. (1992), present knowledge of waves on the sea surface that have wavelengths comparable to those of the radar is poor. Therefore, all scattering calculations may be considered suspect until that knowledge improves. Recently Apel (1994) has proposed a new model of the wave spectrum that attempts to synthesize present knowledge, but scattering calculations, of the type carried out by Rodriguez et al. (1992), also require geometrical modelling of the sea surface that cannot be carried out purely on the basis of a spectral model of the type proposed by Apel (1994). The second reason why any theoretical modeling may prove inadequate is that the radar altimeter onboard software and hardware used to estimate backscattered power may not give the true value of σ^0. To date there have been various unexplained differences between σ^0 values obtained from different altimeters [a 1.6-dB difference was originally noted between *GEOS-3* and Seasat; see Fig. 3 of Fedor and Brown (1982)]. Apart from Topex, all the altimeters flown in space so far have been K_u-band ones and the differences in σ^0 have been adjusted empirically [as have the values for Topex (Callahan et al. 1994b)], but this is clearly unsatisfactory in terms of physical understanding.

To summarize, it seems problematical at the present time to provide a convincing model of backscattered power that will explain the observed differences between the C- and K_u-band values of σ^0. Furthermore, the variations of σ^0 from one K_u-band radar altimeter to another remain largely unexplained. [The one exception is the well-documented offset of 0.7 dB between Topex and Geosat σ^0's, which is due to Topex's allowance for the curvature of the earth and its mean atmospheric correction (Callahan et al. 1994b).] Both aspects of the problem require further investigation and lie beyond the scope of this paper. Consequently, for the purpose of this investigation, an empirically derived relationship between C- and K_u-band values of σ^0 is used.

b. Determination of an empirical relationship

To fully appreciate the different degree to which rain affects K_u- and C-band altimetry, it is helpful to look first at the relationship between their respective normalized backscatters during normal operating conditions. It has been noted that there is an approximately 4-dB difference in values, but their relationship is more complicated than a simple offset. Figure 1 shows a scatterplot of the 1-Hz σ^0 values produced from 80 days of GDR data spanning a year. The details of the data selection are given later.

The main body of Fig. 1 shows a scatter diagram, with three lines appended, indicating the mean and spread (± 1 sd) of K_u-band σ^0's for each C-band value. The bin size used is 0.05 dB, which is smaller than the precision of the instrument, as can be seen from the spikes in the histogram at the top of Fig. 1. The majority of C-band σ^0 values lie in the range 13–20 dB. The sd of values in each bin is also plotted on the top axes, showing that the spread is at a minimum (0.2 dB) for the regime where most of the data exist. The very high backscatter values (>20 dB) are mainly due to contamination by sea ice, with the large scatter about the mean due to the random sampling of specular scatterers. The large spread in values at the low σ^0 (high wind) end is based on a small number of points (around 20 per 0.05-dB bin for C-band values less than 11.5 dB), but from 12.0 to 20.0 dB there are over 800 points per bin.

Various data constraints were examined in producing the definitive version shown in Fig. 1: these will be discussed later, but first a few points are brought out concerning the general form of the main graph. The perceived backscatter at either frequency is highly dependent on the degree of roughness of the sea surface—the rougher the surface, the less directly reflected radiation—which is primarily related to the local wind field. Thus a high degree of positive correlation in σ^0 values is to be expected, as a change in the roughness of the sea surface affects both in the same way. However, due to their different electromagnetic wavelengths, each interacts with a different portion of the spectrum of sea surface height variations, being insensitive to roughness on scales much smaller than this wavelength (Brown 1978). The shorter wavelength K_u-band radar "feels" the effect of the small-scale waves more than the larger wavelength C-band radar. As the short wavelength tail of the wave spectrum contributes greatly to the mean square slope (Jackson et al. 1992), the backscatter at K_u band is less than at C band. However, this effect is not linear with wind speed; this explains why the dark line indicating the mean relationship between C and K_u bands is not a straight line of unit slope.

The degree of scatter about this mean relationship (an rms spread of about 0.2 dB) indicates that other factors than wind are also affecting the σ^0 values. Note the different beamwidths at the two frequencies is not an issue here, provided that severe mispointing does not occur, since the region observed by the altimeter is pulse limited (see Chelton et al. 1989). Some variation may be due to random sampling and instrument noise. At the telemetry stage, the return power levels at K_u and C bands are rounded to the nearest 0.25 dB. With large quantities of data, this rounding has no effect on the mean relationship illustrated in Fig. 1; however, it does make a small contribution (less than 0.1 dB) to the observed scatter about such a line. Taking nine-point running mean averages of the K_u- and C-band σ^0's prior to plotting led to a slight reduction in the spread of points about the mean line, but this was nowhere near the factor of 3 expected if deviations from the mean were uncorrelated between successive records. The scatter must be at least partly due to oceanographic or atmospheric processes that exhibit significant along-track correlations.

As indicated earlier (section 1), rain has a proven effect on σ^0 levels at K_u band. An indication that this is a major feature in explaining some of the scatter in Fig. 1 is that most of the severe outliers (greater than 1 dB from the mean) lie below the mean, corresponding to a *reduction* in K_u values. This point is more clearly demonstrated in the case studies shown in section 4.

The data in the GDR contain a correction for attenuation, calculated as a function of estimated liquid water and water vapor paths [see (2)], as well as *corrected* values for the backscatter at K_u and C bands. Here we have chosen to reverse these corrections and use uncorrected values of σ^0 throughout. We have done this on three grounds.

(i) This paper aims to study the effects of rain on the altimeter data, and it would thus be confusing to use data for which some correction has been made.

(ii) The same correction has been applied to both C and K_u bands, whereas their appropriate values should be somewhat different.

(iii) The correction is set to a default value in cases of extreme rain, leading to a discontinuity in the applied correction (typically of order 0.5 dB) on transits of intense storms.

Figure 1 is the result of a series of studies applying various constraints on data validity and making two particular assessments of their suitability: does it encourage the omission of outliers such that the remaining data are more uniform and hence have lower spread in values, and does it still facilitate comparisons over a wide range of σ^0 values? The results of this iterative process are described below.

The data shown in Fig. 1 are for points with LWP < 0.2 mm. Since attenuation of K_u band could be significant for high liquid water contents, the plotting exercise was also performed with a constraint that only points for which the LWP was less than 0.01

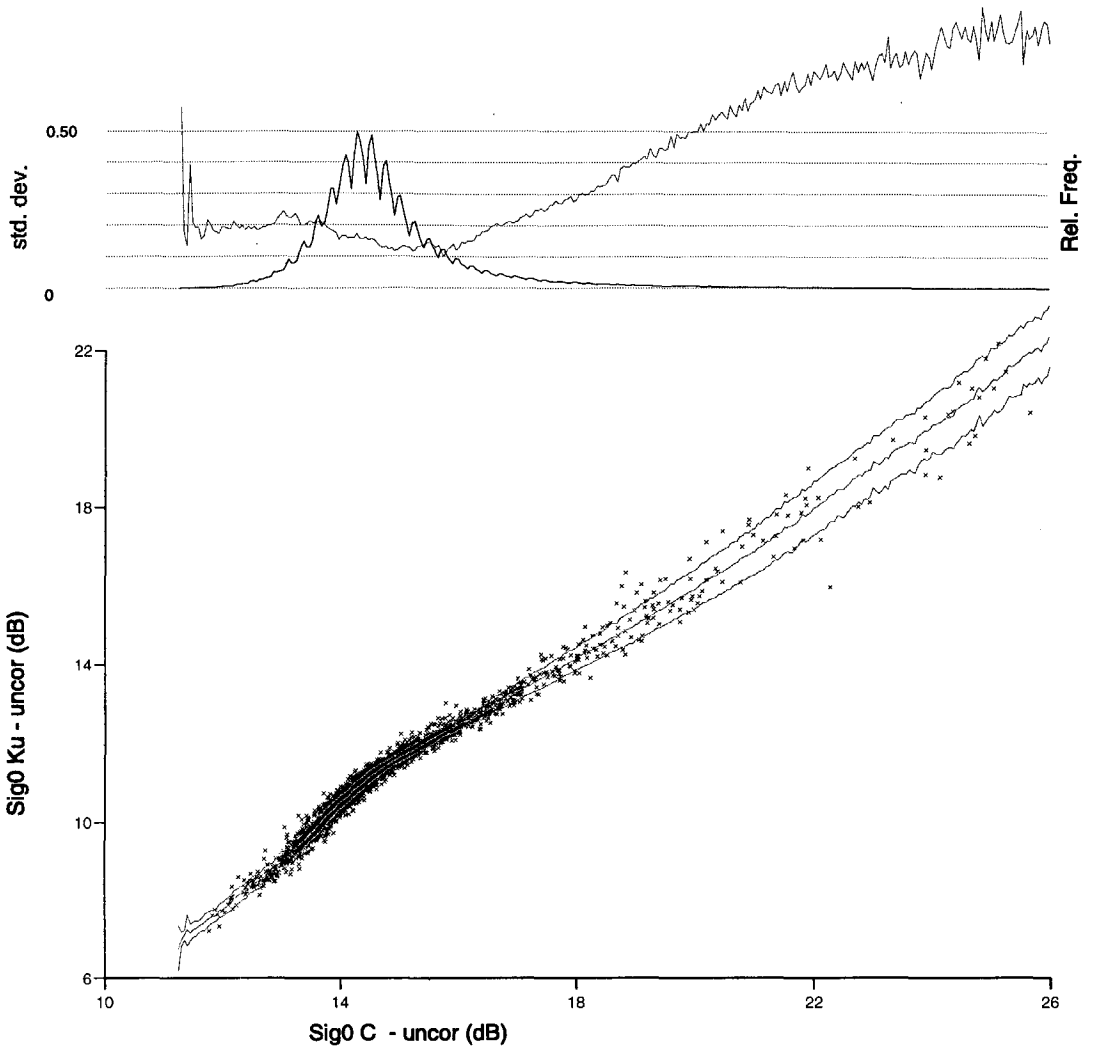

FIG. 1. A scatterplot of the uncorrected 1-Hz σ^0 values at the two frequencies of the Topex altimeter. Here 80 days of data (cycles 11 and 12, 21 and 22, 29 and 30, 39 and 40) spanning all four seasons were used, with records having LWP > 0.2 mm discarded. The three lines on the main plot show mean and spread (± 1 sd) for 0.05-dB bins. The gray line in the upper plot gives the standard deviation in each bin as a function of C-band σ^0, while the dark line indicates their relative frequencies of occurrence. Only a subset of the points is plotted for clarity, but the statistics were calculated using all the data.

mm were used. This did lead to a slight reduction in the sd in the most populous region of data; however, very few "dry air" points were found in the low-σ^0 regions typical of intense storms. Since part of this study was to be of altimeter transits of intense events, the absence of a clear relationship in the low-σ^0 regime could not be accepted, so the constraint was relaxed to a liquid water path of 0.2 mm. Such a relaxation had little effect on the mean, except for at very low σ^0's (C-band values less than 13 dB). This indicates that those extra included points lay both sides of the curve. An additional editing restriction of only accepting data within 1 dB of the mean was tested, but its effect was minuscule for C-band $\sigma^0 < 20$ dB, indicating that few such outliers existed.

Figure 1 was produced from four 20-day segments of data, covering all the seasons. The data have not been corrected for the long-term secular variation, estimated from calibration measurements (Callahan et al. 1994a). Slight differences occur between the means for different seasons, with shifts in the mean line of about 0.1 dB in places from the annual mean. Applying the suggested secular correction made little difference. Given that this analysis is for data with a conservative LWP limit of 0.2 mm (the rain flag is set above 1 mm), this is unlikely to be due to seasonal variations in the prevalence of rain, even though many rain events are

smaller than the TMR footprint. Changing the LWP limit to 0.01 mm made little difference to the results, suggesting that the effect of small cellular precipitation is minimal. This slight seasonal variation may be due to some other process that affects σ^0 values and that does itself vary during the course of a year.

From the mean curve in Fig. 1, a simple piecewise monotonic function is created for rescaling of C-band σ^0's to the equivalent values at K_u band: its form is given in Table 1. These rescaled C-band σ^0's are used in all the figures referred to in section 4, as then they may be conveniently plotted on the same scale as the K_u values. The term "sigma0 anomaly," $\Delta\sigma^0$, is introduced to refer to the deviation of the K_u-band σ^0 from its expected value given the C-band σ^0, that is,

$$\Delta\sigma^0 = \sigma^0(K_u) - f[\sigma^0(C)], \qquad (4)$$

where $f(\ )$ is the function described in Table 1. Note, it is expected that rain will cause more attenuation at K_u band than C band, so the associated $\Delta\sigma^0$ value will be negative. Given that the rms spread of points about the mean is typically less than 0.2 dB, $\Delta\sigma^0$ values whose magnitude exceeds 0.5 dB may be regarded as significant.

TABLE 1. Function used for rescaling C-band σ^0's to equivalent value for K_u band. The function has been defined up to 26 dB based on data shown in Fig. 1, although most values greater than 20 dB are probably due to sea ice. It is based very closely on the mean (middle curve) plotted in Fig. 1. An extrapolation is indicated for $\sigma^0 < 13$ dB, based on data between 12.2 and 13 dB; C-band values below 12 dB are very rare.

$f(\sigma^0) =$	$8.99 + 1.19\,(\sigma^0 - 13.0)$,	$\sigma^0 < 13.0$ dB
	$8.99 + 1.52\,(\sigma^0 - 13.0)$,	$\sigma^0 \in \{13.0$ dB, 14.0 dB$\}$
	$10.51 + 1.21\,(\sigma^0 - 14.0)$,	$\sigma^0 \in \{14.0$ dB, 14.7 dB$\}$
	$11.36 + 0.89\,(\sigma^0 - 14.7)$,	$\sigma^0 \in \{14.7$ dB, 15.7 dB$\}$
	$12.25 + 0.72\,(\sigma^0 - 15.7)$,	$\sigma^0 \in \{15.7$ dB, 16.2 dB$\}$
	$12.61 + 0.86\,(\sigma^0 - 16.2)$,	$\sigma^0 \in \{16.2$ dB, 19.4 dB$\}$
	$15.36 + 0.96\,(\sigma^0 - 19.4)$,	$\sigma^0 \in \{19.4$ dB, 21.0 dB$\}$
	$16.90 + 1.07\,(\sigma^0 - 21.0)$,	$\sigma^0 \in \{21.0$ dB, 24.2 dB$\}$
	$20.31 + 1.11\,(\sigma^0 - 24.2)$,	$\sigma^0 \in \{24.2$ dB, 26.0 dB$\}$
	undefined,	$\sigma^0 > 26.0$ dB

4. Case studies

The process described in section 2c selected many cases where the K_u-band σ^0 values underwent a rapid change. Not all of these were caused by high precipitation rates. Examples are shown here of both wind- and rain-induced variations, indicating how such events may be clearly distinguished by their different effects on the altimeter and radiometer signals.

a. The effect of wind

Figure 2 is an example of how well the K_u- and C-band backscatter values compare after rescaling. This particular plot is of an altimeter transit across what appears to be a strong atmospheric front in the Southern Ocean, southwest of Australia. The range of σ^0 values shown (8–12 dB) spans the most frequently occurring values for K_u band. After the rescaling specified in Table 1, the C-band values are shown not only to cover the same range but to agree in detail with the collocated K_u values, showing even small spatial features in common. This is not surprising given the generally low (0.2 dB) scatter of points about the defined line. The σ^0 profile at K_u band is readily interpreted as a moderate wind field across the region (9 dB corresponds to a U_{10} of 6 m s^{-1}), with strong localized winds of up to 15 m s^{-1} over a region about 100 km wide near 57.5°S.

The significant wave height measurements H_s at the two frequencies also agree well (this is nearly always true, so, for clarity, only the K_u-band values are plotted in Figs. 2–7). The H_s curve shows a sharp step from 4.5 m south of 58°S to a value of 7 m by 57.5°S, and returning to 5 m to the north of the front. This is consistent with strong local winds around 57.5°S. The other lines on the plot show the values for σ_h (the standard deviation of the 20 height measurements in each 1-s record) and LWP. The LWP values are low (never more than 0.2 mm), indicating that the TMR shows no evidence of rain. The σ_h values are around 0.02 m (typical of the high quality Topex altimeter) for most of the region.

b. The effect of rain

The second example (Fig. 3) shows an altimeter transit of a simple rain event. The figure shows the altimeter profile as it travels southward across the mid–equatorial Pacific, a region traversed by the intertropical convergence zone (ITCZ), which is known for its intense rainfall (see section 6). Once again, the wave heights and rescaled σ^0's show good general agreement, with H_s dropping from 3 to 1.5 m to the south, and σ^0 values generally in the region of 10–12 dB, implying winds in the range 6–13 m s^{-1}. However, between 12° and 13°N this simple picture of gradually changing H_s and σ^0 is disturbed. The backscatter at K_u band plummets to 8 dB, while no equivalent change occurs at C band. The 2.3-dB difference is readily explained as attenuation due to a high liquid water content of the atmosphere. It is noted that the LWP value, derived from totally independent instrumentation, undergoes a rapid increase from less than 0.3 to 1.5 mm. This feature does not necessarily line up perfectly with the dip in σ^0 values, as radiometer-derived measurements will respond more to features a little off the subsatellite track than the altimeter does, due to the TMR's larger footprint. The σ_h values stay low, with a small spike (σ_h = 0.06 m) on the edge of feature at 12.4°N and two larger spikes at 10° and 8.6°N; the latter coinciding with a small drop (~1.5 dB) in σ^0 at K_u band and a large spike in H_s at both K_u and C bands. The rain flag, based entirely on radiometric measurements, is set only for the central portion of the main rain cell (12.5°–13°N).

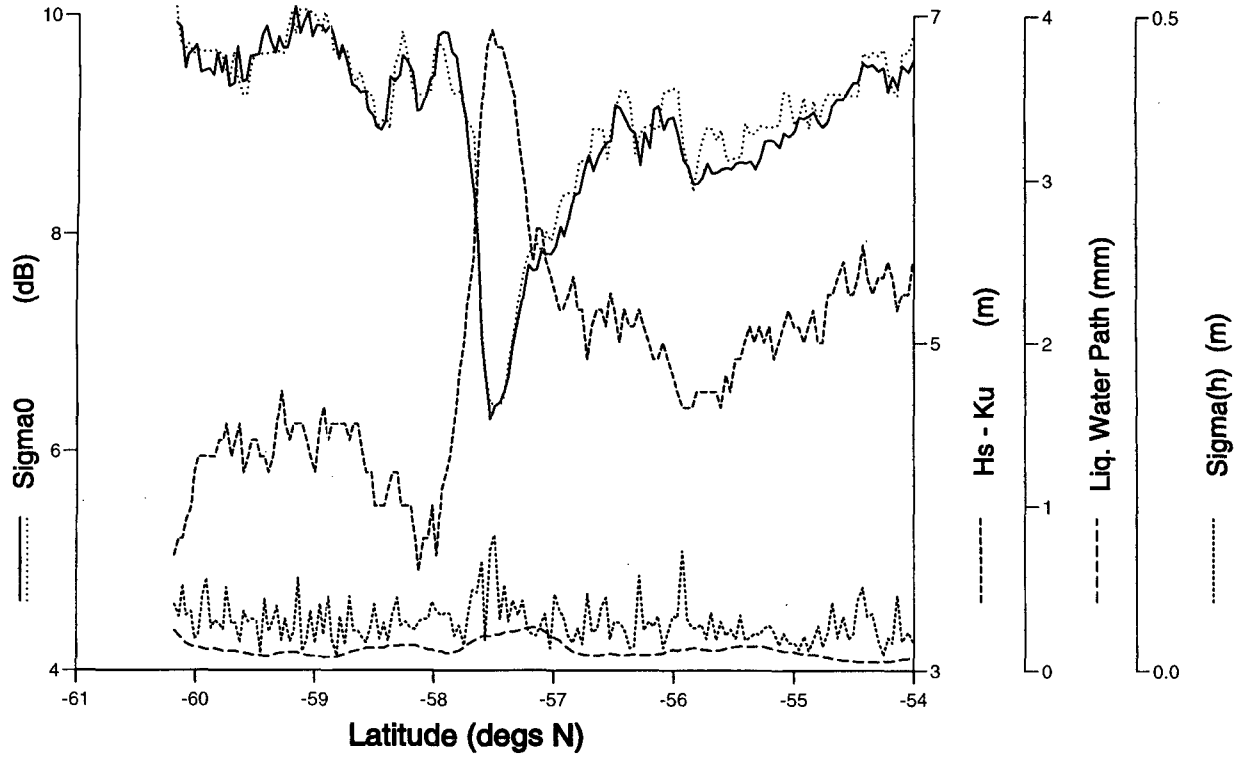

FIG. 2. Ascending altimeter profile (cycle 33, track 225) for Topex crossing a region of the Southern Ocean to the southwest of Australia. The σ^0 values at K_u band are shown by the solid line, with the rescaled C-band values (given by the lightly dotted line) plotted on the same axis. Also shown are the significant wave height H_s (dashed line), σ_h (heavily dotted line), and the derived LWP (long-dashed line). A bar along the x axis (when present) indicates that the rain flag is set. Note for the purpose of display, all data are plotted, including some flagged as untrustworthy.

c. An extreme event

Figure 4 shows an altimeter profile just to the southeast of Japan; the derived geophysical fields are consistent with this being a section across a typhoon. Many of the features are similar to that shown in Fig. 3—agreement of both estimates of wave height across the whole picture and good agreement of the rescaled σ^0 values for the region of low LWP at the periphery of the displayed section.

However, this is an extreme event, with the TMR-derived LWP estimate exceeding 2 mm (a rare occurrence) and the rain flag (bar along the x axis) being set for all data between 30.2° and 33.9°N, an extent of 400 km. Near the center of the typhoon, the backscatter values at K_u band decrease to well below 2 dB, which if caused by wind alone would imply extreme winds. [Most algorithms relating σ^0 to wind speed are not defined below 7 dB because of the paucity of calibration data for such extreme conditions (see Witter and Chelton 1991; Young 1993).] A large spike in H_s occurs near 31°N. Note, to illustrate the effect of rain on the altimeter, all points are plotted irrespective of flagging.

The values for σ_h and σ_{H_s} (standard deviation of 10-Hz H_s estimates) are larger near the center of the typhoon, but this is consistent with the increasing wave height, which affects the noise levels of both measurements. A plot (not shown) of the waveform-derived attitude shows extreme behavior here, fluctuating abruptly from about 0.1° to the default value of 2.55°, indicating that the waveforms cannot be used to determine attitude information. This is because, according to the standard Brown model that makes no allowance for rain effects, the attitude of an altimeter, that is, its mispointing from nadir, may be estimated from the slope of the trailing edge of the waveform. However, analysis for *ERS-1* (GQS) has shown that the slope of this region is particularly sensitive to the presence of rain, both in the center and at the edge of the altimetric footprint.

There is also a secondary region of attenuation at 27.5°N, with the K_u-band value 4 dB lower than the rescaled C-band σ^0. Corresponding spikes of 1 m can be seen in H_s, along with the LWP values in excess of 1 mm. This feature is the result of a rainband at some distance from the center of the storm.

d. Enhanced backscatter

Earlier studies (Srokosz and Guymer 1988; GQS) had shown the existence of regions, often on the edge

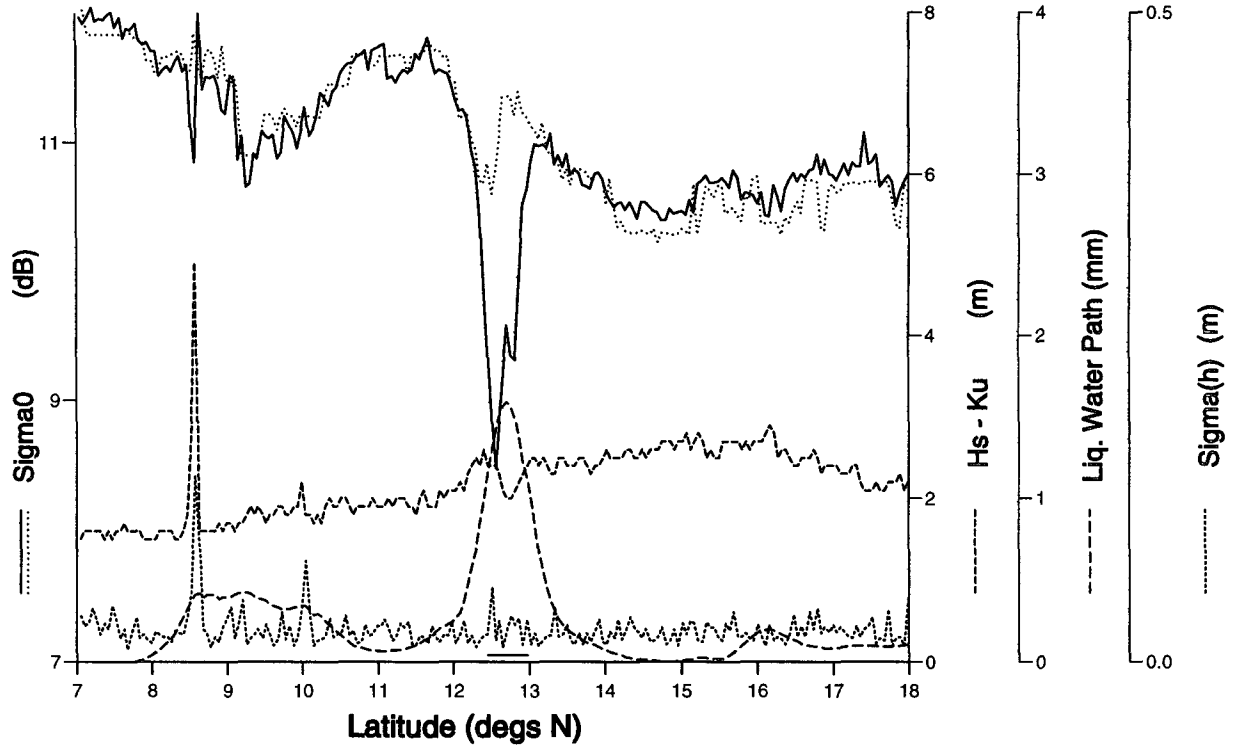

FIG. 3. Descending transit (cycle 33, track 056) of mid-equatorial Pacific; plot characteristics as for Fig. 2.

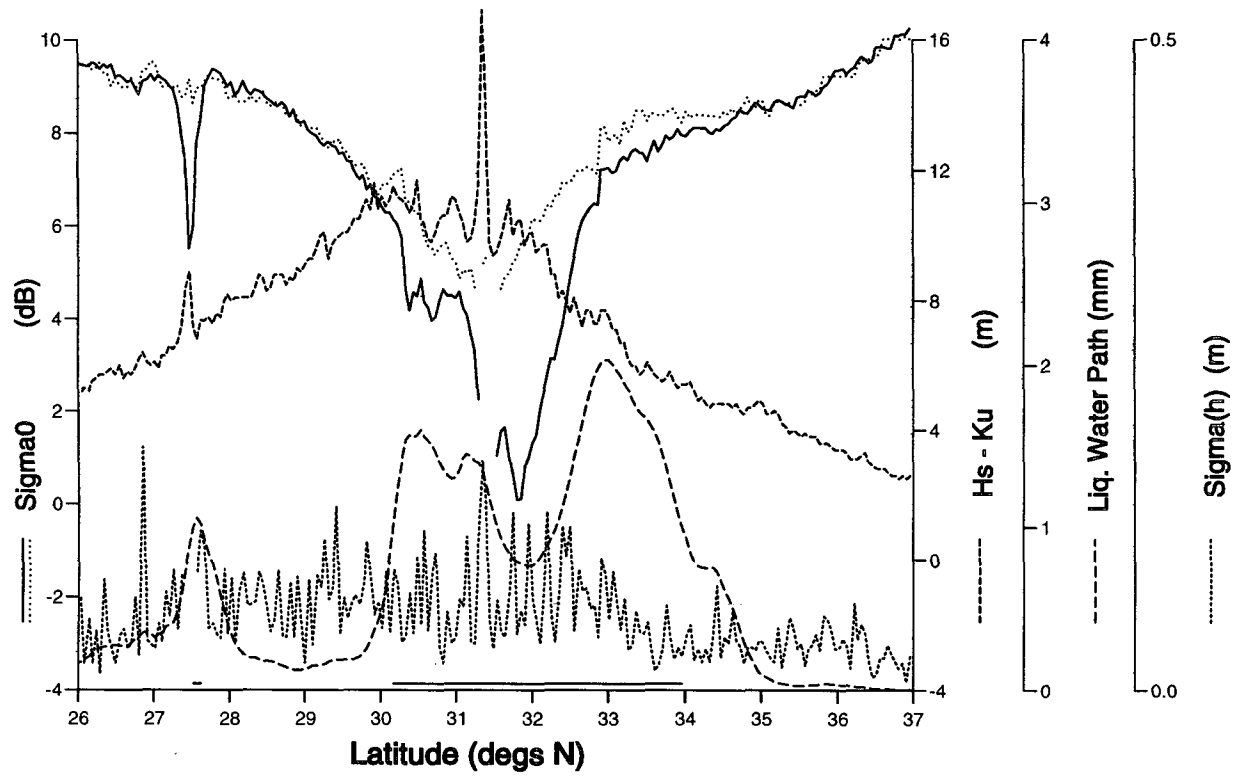

FIG. 4. Descending transit (cycle 38, track 060) of northwest Pacific to southeast of Japan; plot characteristics as for Fig. 2.

of rain events, where the K_u-band σ^0 values appeared higher than the "background" level. Such regions of *enhanced backscatter* could be explained by light rain on the sea surface damping the small-scale ripples (Tsimplis and Thorpe 1989), which give rise to the reflection of the radar pulse. It was not easy to find unambiguous examples for *ERS-1;* for Topex, the task appears harder. However, it is an important challenge, since through comparison of the effect at two different frequencies one may learn more about the processes involved. Figure 5 shows a possible example of enhanced backscatter.

The altimeter section depicted is for a transit of the southwestern Atlantic Ocean. A region of high liquid water content is shown between 43° and 39°S, with the K_u-band σ^0 values maintaining an approximately −0.6-dB offset from the rescaled C-band ones across the whole region. The average wind speed across the region is 16 m s^{-1}, with the wave height peaking at 7 m on the northern edge of the rain area. Just to the north of this (around 39.5°S), the σ^0 values at both frequencies are 0.5 dB higher than occur farther north. This may tentatively be explained by enhanced backscatter affecting both frequencies to a similar extent.

e. A complex example

A more complex case is shown in Fig. 6 to indicate that attenuation does not occur in totally isolated events. A broad region of moisture (indicated by the LWP profile) spans some 400 km of equatorial ocean to the southwest of India. The LWP profile gives some indication of structure to the levels of liquid water; this is emphasised by the more rapidly varying response of the altimeter. At such low wave heights, the footprint of the altimeter for a 1-s average is 7 km across (Chelton et al. 1989), whereas the TMR brightness temperatures are all smoothed to the resolution of the broadest, which corresponds to a footprint of 42 km. Thus, the altimeter shows much smaller-scale variations in atmospheric liquid water content than the TMR does. Additionally, the altimeter can respond to a wider range of rain rates than the TMR.

In detail, Fig. 6 shows four narrow bands of attenuation (1.5°, 2.3°, 3.1°, and 4.8°N), with the LWP profile coalescing the middle two features into one of very high LWP. Two of the features have associated H_s anomalies, while all four of the features have corresponding spikes in the σ_h values.

f. Inverse behavior

Discussion so far has been of good general agreement between K_u- and C-band backscatters values, with departures from such being due to the greater attenuation by liquid water of K_u than C band. Figure 7 shows a counter example, where for a significant interval, the K_u values are higher than those of the rescaled C band.

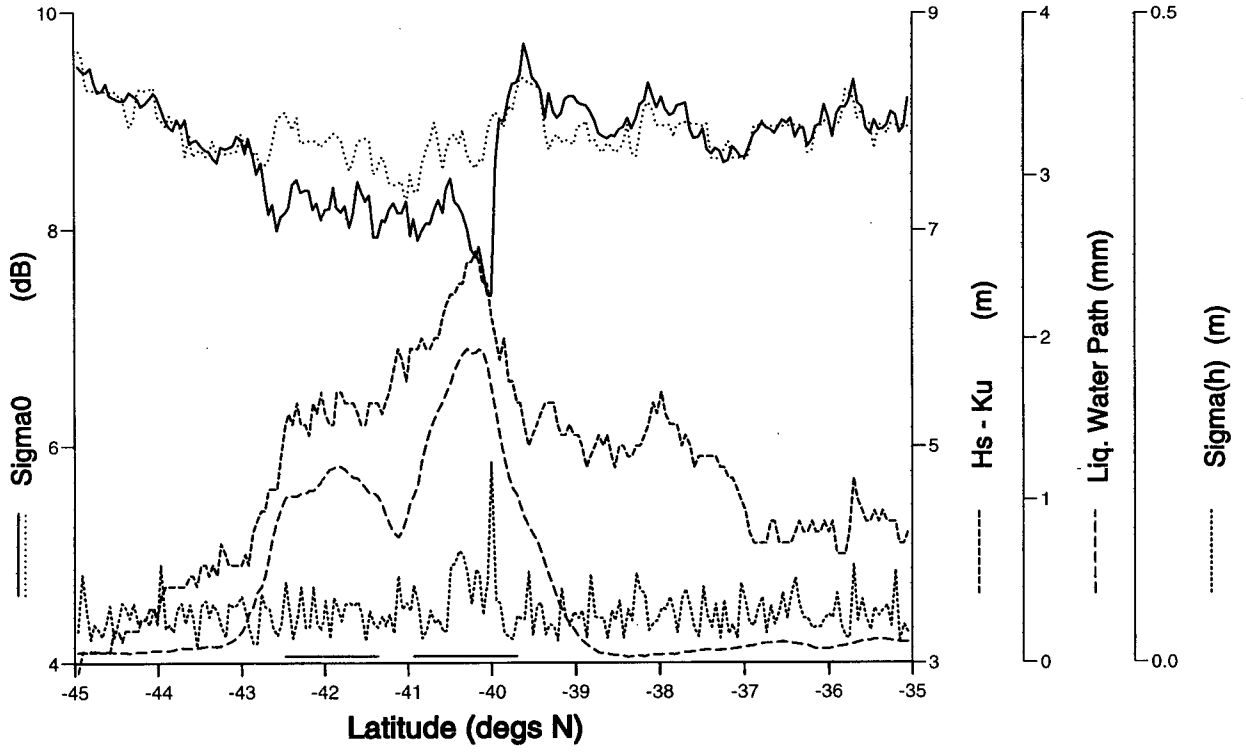

FIG. 5. Descending transit (cycle 36, track 076) of southwest Atlantic; plot characteristics as for Fig. 2.

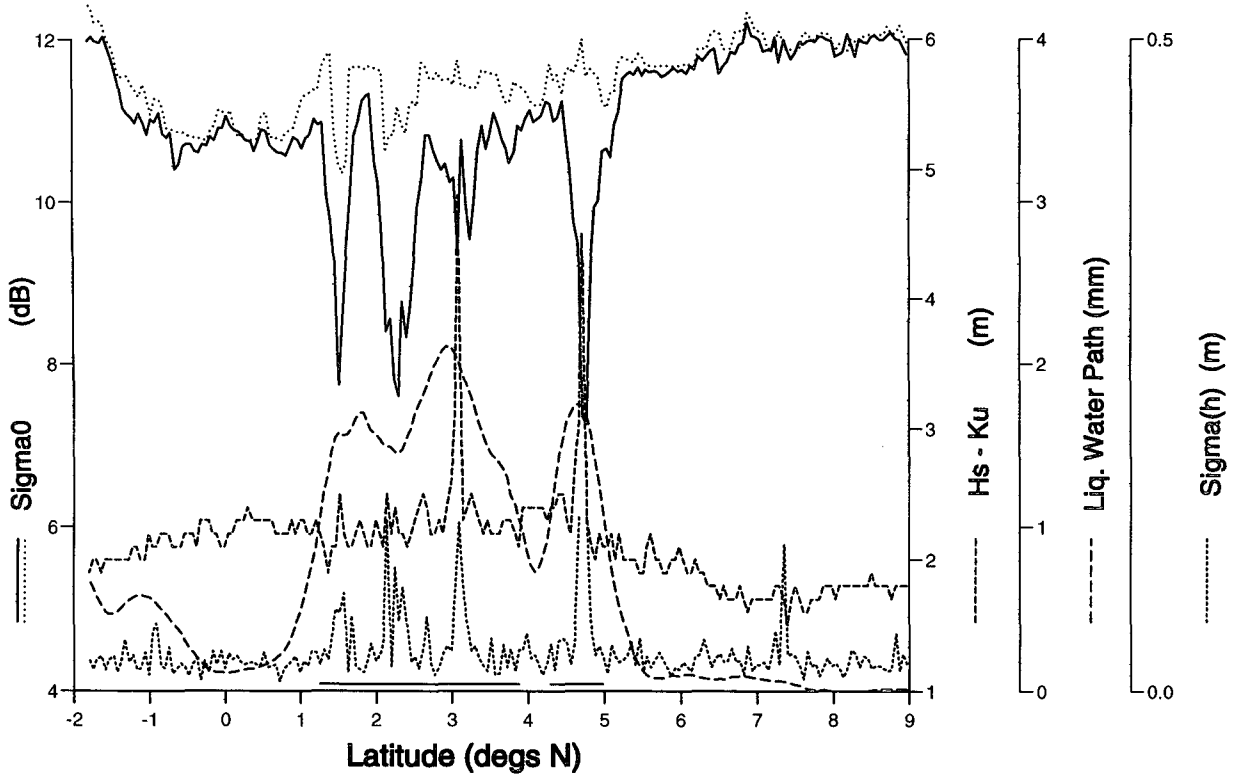

FIG. 6. Descending transit (cycle 37, track 016) of equatorial Indian Ocean to southwest of India; plot characteristics as for Fig. 2.

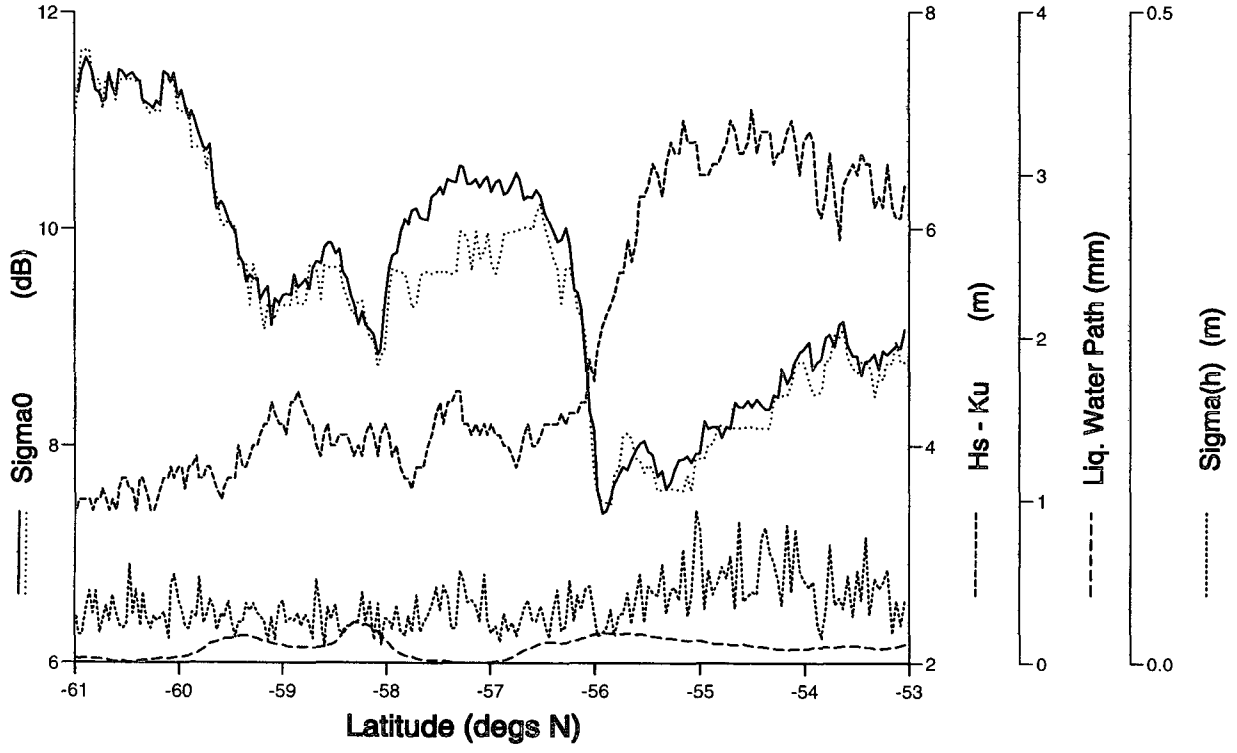

FIG. 7. Descending transit (cycle 33, track 218) of Southern Ocean, to the southwest of Australia; plot characteristics as for Fig. 2.

Over the interval 57.9°–56.5°S, there is a positive offset of the K_u values of around 0.4 dB. Although much smaller in magnitude than the rain-related attenuations, this is well above the noise level of σ^0 measurements, and its occurrence in a well-defined interval indicates the effect of some other atmospheric or oceanographic phenomenon. The example shown is from the Southern Ocean to the southwest of Australia; section 6c explores the global distribution of such events.

5. Comparison of altimeter and radiometer measurements

A direct comparison between altimeter σ^0 fluctuations and in situ rain measurements is difficult because of the problem in siting rain gauges at sea. Here we compare the altimeter observations with another indicator of rain at sea: high brightness temperatures as observed by the TMR. Although the altimeter data shows attenuation of radar pulses (principally at K_u band, 13.6 GHz), while the radiometer measures emission at higher frequencies (18, 21, and 37 GHz), some correlation in their observations may be expected.

a. Use of radiometers to detect rain

A series of passive microwave radiometers has been flown in the last 20 years, including the SMMR (Scanning Multichannel Microwave Radiometer) present on Seasat and *Nimbus-7* and the SSM/I (Special Sensor Microwave/Imager) flown on the Defense Meteorological Satellite Program series of satellites. Through extensive ground-truthing campaigns, using rain gauges and local ground-based radar, attempts have been made to relate the spaceborne microwave observations to rain rate and fractional rain coverage (Petty and Katsaros 1990; Petty and Katsaros 1992). The data, however, do not yield a simple monotonic relationship between rainfall and brightness temperature at any particular frequency, as the emissions at 18 GHz reach a saturation level for rain rates in excess of around 20 mm h^{-1}, with the required rain rate for saturation being lower for the higher frequencies (Wilheit et al. 1977; Wilheit and Chang 1980).

There has been no validation campaign for the TMR, but all of its frequencies are similar to those of the SMMR instrument. However, the SMMRs produced dual-polarization swath images by scanning at 50° to nadir, whereas TMR is only directed perpendicular to the sea surface. Estimates of the atmospheric variables from the radiometer data [such as (1), (2)] are based on the assumption that TMR's performance is similar to that of SMMR.

b. Global comparisons of simultaneous altimeter and TMR data

The total attenuation at K_u band is hard to determine accurately. For simple sharp dips in σ^0, the magnitude of the feature may be taken as the degree of attenuation. However, the number of cases that are simple are relatively few. Here we assume the rescaled C-band values give an indication of what the K_u value would be in the absence of atmospheric liquid water. The observed departure from this, $\Delta\sigma^0$ [see (4)], may be used as a good estimate of the attenuation at K_u band, as that at C band is much smaller.

Figure 8 is a scatter diagram of the brightness temperatures measured by the radiometer at 37 GHz, with the coincident $\Delta\sigma^0$ values from the altimeter. The dark line in the upper plot emphasizes that the majority of points have K_u-band and rescaled C-band σ^0's agreeing within 0.5 dB, which is consistent with the degree of scatter shown in Fig. 1. Figure 8 is based on the same 80 days of data as Fig. 1 except that all data with C-band σ^0 above 20 dB were discarded, but none were discarded on grounds of their LWP value. The data are grouped in 0.2 dB bins for calculation of mean and sd of coincident brightness temperatures. On the left-hand side of this plot, these statistics show sampling noise as for intervals below −3.0 dB there are less than 100 data points per bin; whereas for intervals to the right of −2.0 dB, there are more than 500 points per bin.

For $\Delta\sigma^0 \geq 0$ dB, the mean brightness temperature at 37 GHz, T_b (37 GHz), is about 165 K, with an rms spread of about 10 K. As expected, significant negative anomalies are associated with much higher brightness temperatures; a $\Delta\sigma^0$ of −0.6 dB typically corresponding to a temperature of 190 K. Yet lower (i.e., more negative) sigma0 anomalies have correspondingly higher values of T_b (37 GHz); however, by a value of −2.4 dB, the mean of T_b (37 GHz) has peaked at about 245 K. The rms spread of T_b (37 GHz) is greatest in the range −1.2 to −0.6 dB. The points for which the rain flag have been set (indicated by circles) lie predominantly at the top of the plot since they correspond to high values of LWP or T_b (37 GHz).

Similar plots can be produced for the other TMR channels; a comparison of all three is shown in Fig. 9. The quiescent temperature for typical nonraining conditions is about 135 K at 18 GHz, about 155 K at 21 GHz, and about 165 K at 37 GHz. Regarding the $\Delta\sigma^0$ term as a proxy for the actual rainfall rate, it can be seen that the highest TMR frequencies respond most rapidly to an increase in rain rate (more negative $\Delta\sigma^0$). The mean curves for all these channels peak at about 240 K, showing no greater brightness temperatures for yet more intense rain. The channel with the greatest response to small levels of rain is thus the first to reach a saturation value. Wilheit et al. (1977) observed similar behavior in comparing ground-based 19- and 37-GHz radiometers against rain data. A similar plot for the LWP estimate [defined in (1)] is shown in Fig. 10. Its saturation occurs for a $\Delta\sigma^0$ of about −1.6 dB.

At moderately high rain rates, brightness temperatures reach a saturation level as the rain layer becomes optically thick; that is, the added emission of micro-

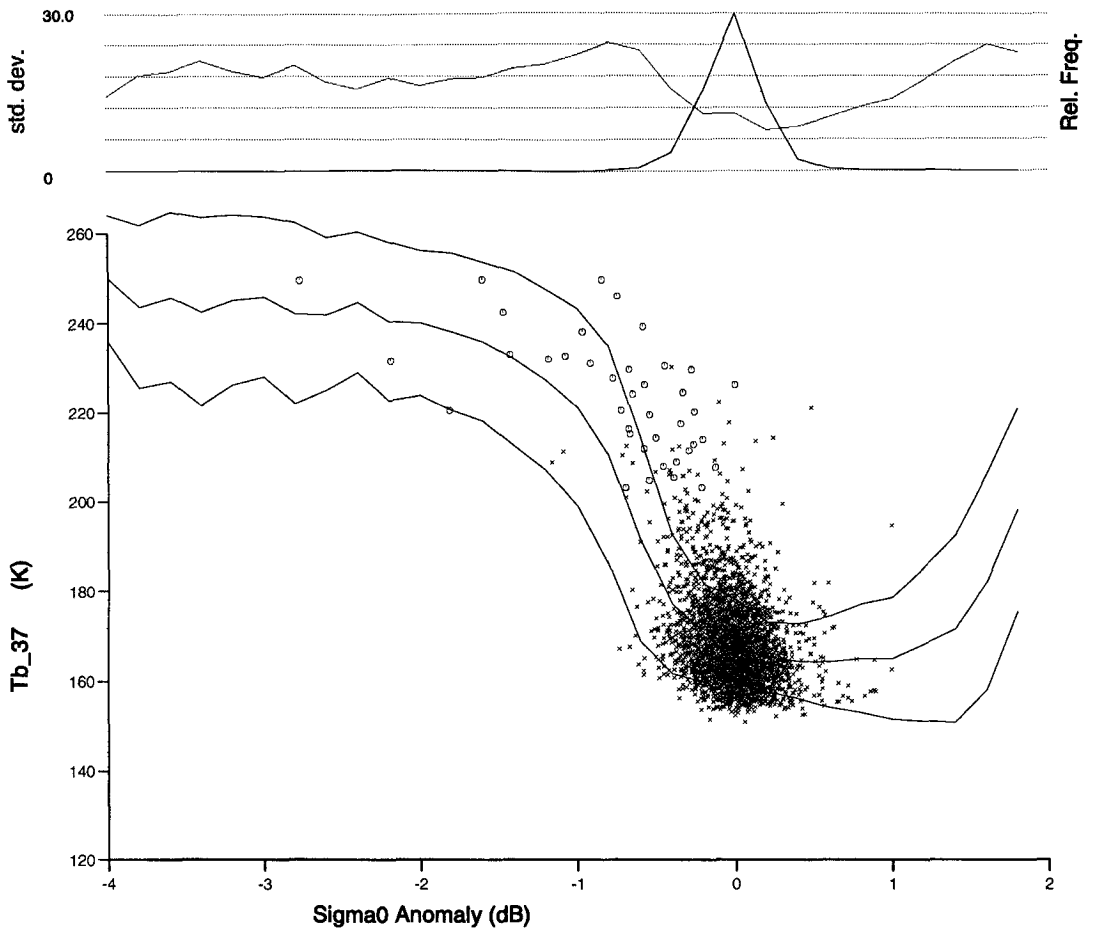

FIG. 8. Scatterplot of radiometer determined brightness temperatures at 37 GHz with coincident sigma0 anomaly values. Data are from the same 80-day period as Fig. 1, but with records having $\sigma^0(C) > 20$ dB excluded and the previous restriction on LWP waived. The added lines show the mean and spread (± 1 sd) for each 0.2-dB bin. Of the subset of points actually plotted, those marked by a circle correspond to occasions when rain flag was set (see section 2b); crosses show when it was not set. On the top axis, the darker line gives the relative frequency, and the lighter one the standard deviation.

waves by the top layers is balanced by their absorption of emissions from lower down. However, the sigma0 anomaly, $\Delta\sigma^0$, being the attenuation of a passing radar pulse integrated over the whole atmospheric column, shows no saturation. Thus, the steep linear slopes between -1 and 0 dB in Figs. 8–10 are due to both sensors responding to an increase of liquid water in the *total* atmospheric column. For much more intense rain, the $\Delta\sigma^0$ values are believed to increase approximately proportionally, while the TMR "sees" only the top of the clouds and yields the saturation value. By extrapolation, it seems likely therefore that a $\Delta\sigma^0$ of -3 dB corresponds typically to a real liquid water path of 5 mm.

In order to correct other K_u-band altimeters, it would be useful to be able to adjust σ^0 values according to a correction estimated from coincident radiometer data. Then realistic unbiased wind speeds could be inferred in most conditions. Such a correction would be applied to the supplied K_u-band σ^0's as below:

$$\sigma^0(K_u)' = \sigma^0(K_u) + g(\theta), \tag{5}$$

where θ is a measurement from the radiometer, either a brightness temperature at one frequency or a combination of them such as LWP, and $g(\theta)$ is a smooth functional representation of the mean sigma0 anomaly associated with a radiometer measurement of θ. The problem with implementing such an inversion is the scatter observed in plots such as Figs. 8 and 10. An examination of the σ^0 correction supplied on the GDR shows that for moderate rainfall its value is about 60% of that derived from our analysis. However, as for Figs. 8 and 10, there is a lot of scatter of the data, and the supplied correction is useless for strong precipitation events since it reverts to a default value in such cases.

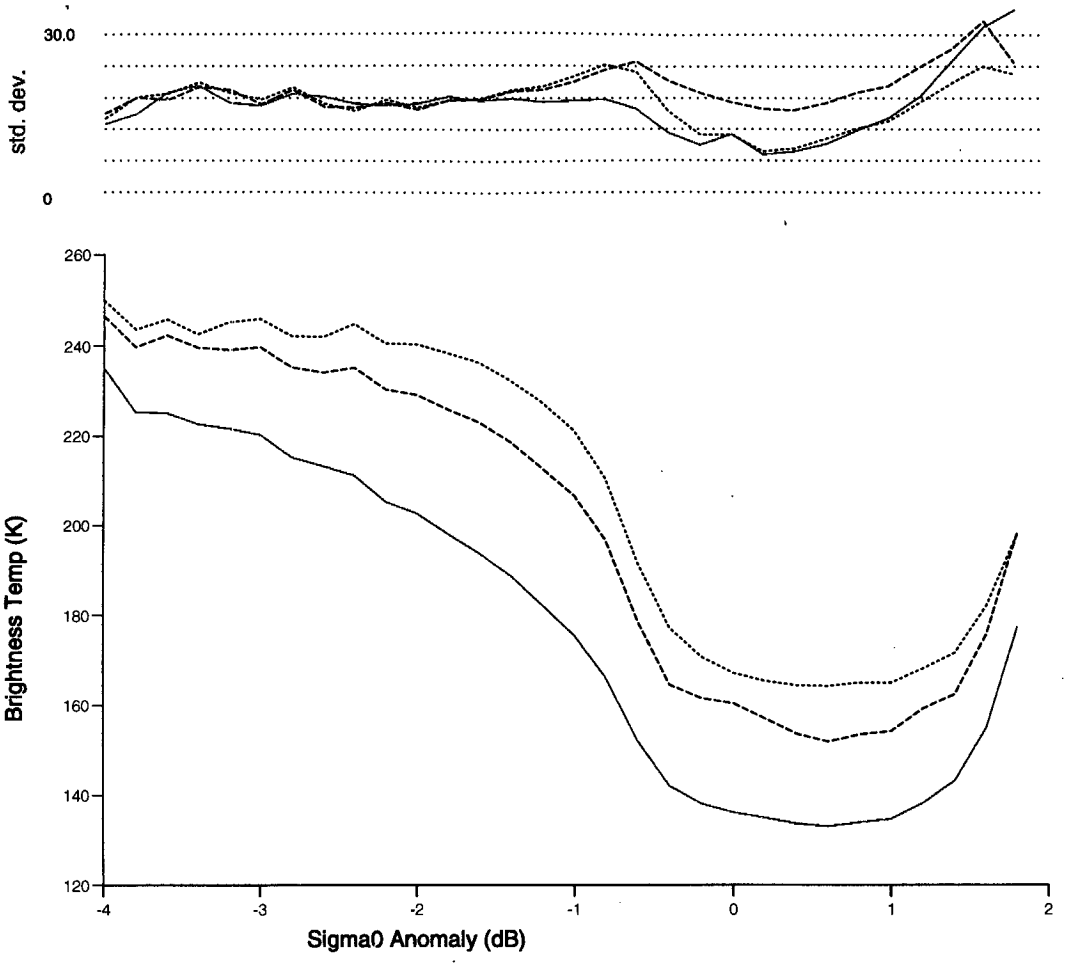

FIG. 9. Comparison of mean brightness temperature curves for all three radiometer channels: 18 GHz (solid), 21 GHz (dashed), 37 GHz (dotted).

There are several possible reasons for such scatter. First, there is instrumental error and variation—this effect is fairly small, with the altimeter registering power levels to within 0.25 dB and the TMR having a stated accuracy of less than 1 K (Callahan 1993). Second, there is the fact that the instruments respond to slightly different phenomena. Third, the two instruments have different effective footprints, with the TMR's being around four times bigger than that of the altimeter. This may be a major cause of the large spread of points.

6. Geographical distribution and seasonal change

a. Location of anomalous altimeter data

It is instructive to examine how the anomalies are distributed over the world ocean. First occasions of rapid change in K_u-band σ^0 have been plotted for March–April 1993. The resulting map (Fig. 11) shows 101 jumps, with some clustering into particular regions, but the number of points is insufficient to draw conclusions of any significance. (Figure 11 contains additional information that will be discussed in Section 6b.) A similar analysis by GQS for *ERS-1* at the same time of year produced a similar number of jumps, but of those a smaller proportion were off Antarctica and more occurred in the tropical Pacific. It was found that a much greater number of anomalies result if the selection is made on $\Delta\sigma^0$ instead of sudden jumps in K_u. This allows more detailed analysis of any spatial variations. Figure 12a shows the location of all points where the rescaled C-band values exceed K_u values by more than 0.5 dB during March and April 1993. (An additional restriction that the C-band σ^0's must be less than 20 dB has also been imposed in order to eliminate sea ice.) From the discussion and results presented earlier in the paper we expect the plotted points to be associated with rain events that cause greater attenuation at the higher frequency.

The anomalies are not randomly distributed but lie in distinct zones. An obvious feature is the east–west band running across all oceans just north of the equator. This

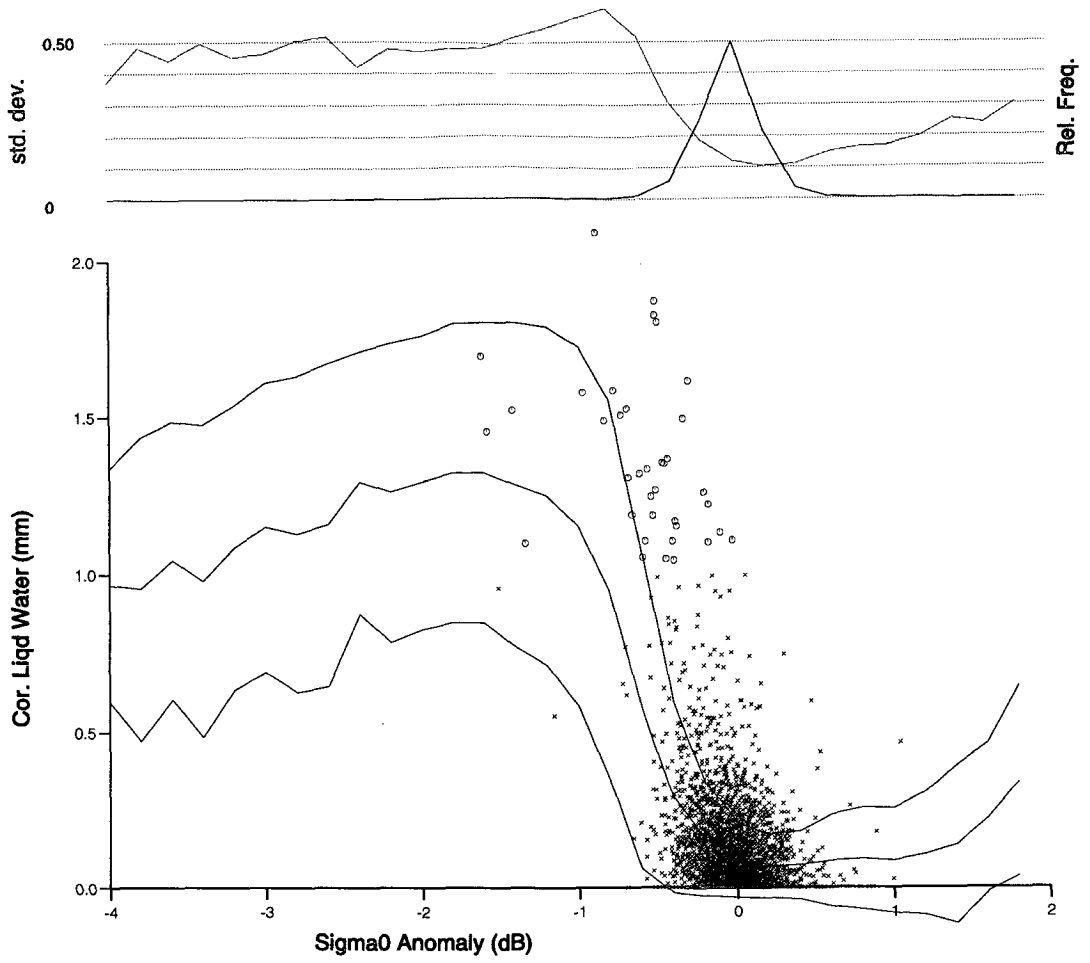

FIG. 10. Same as Fig. 8 but for calculated liquid water path [see Eq. (3)].

is close to the mean position of the ITCZ, which, at this time of year, is at its farthest south. A little farther from the equator, in the region occupied by the subtropical anticyclones, there is a much lower density of anomalies, particularly in the Southern Hemisphere. In the South Pacific this "drier" area is confined to a triangle on the eastern side of the basin by a band of anomalies running southeastward from Indonesia. This corresponds to the location of the South Pacific convergence zone (SPCZ). The South Atlantic shows some evidence for a similarly oriented feature, but this appears restricted by the Atlantic's narrow width relative to the Pacific. At midlatitudes there is a higher occurrence of anomalies in the unsettled westerly airstreams.

There is a similar pattern during the opposite season, September–October (Fig. 12b). Slight differences that are apparent on comparison are the smaller anomaly-free areas in the northern subtropics (and the reverse in their Southern Hemisphere counterparts), the more distinct SPCZ, and the northward displacement of the equatorial band, associated with the known seasonal migration of the ITCZ. Also observable is a sharp southern limit in the Southern Ocean due to the elimination of values over ice. In March–April, the ice edge lies mainly beyond the southern limit of Topex's coverage (66°S).

b. Comparison with independent rainfall climatology

How closely do the altimeter anomaly distributions relate to the spatial variation of precipitation? To answer this question, we have examined published monthly rain accumulations produced by the Global Precipitation Climatology Centre using a combination of infrared sensors, microwave radiometers, and ECMWF model predictions (GPCC 1993). Data are only available for 1987 and 1988; we have produced plots of the mean monthly rainfall for the appropriate parts of the year (Figs. 13a and 13b). Visual inspection shows there is a strong similarity between areas of high precipitation and clustering of anomalies. During September–October, the northward extension of high pre-

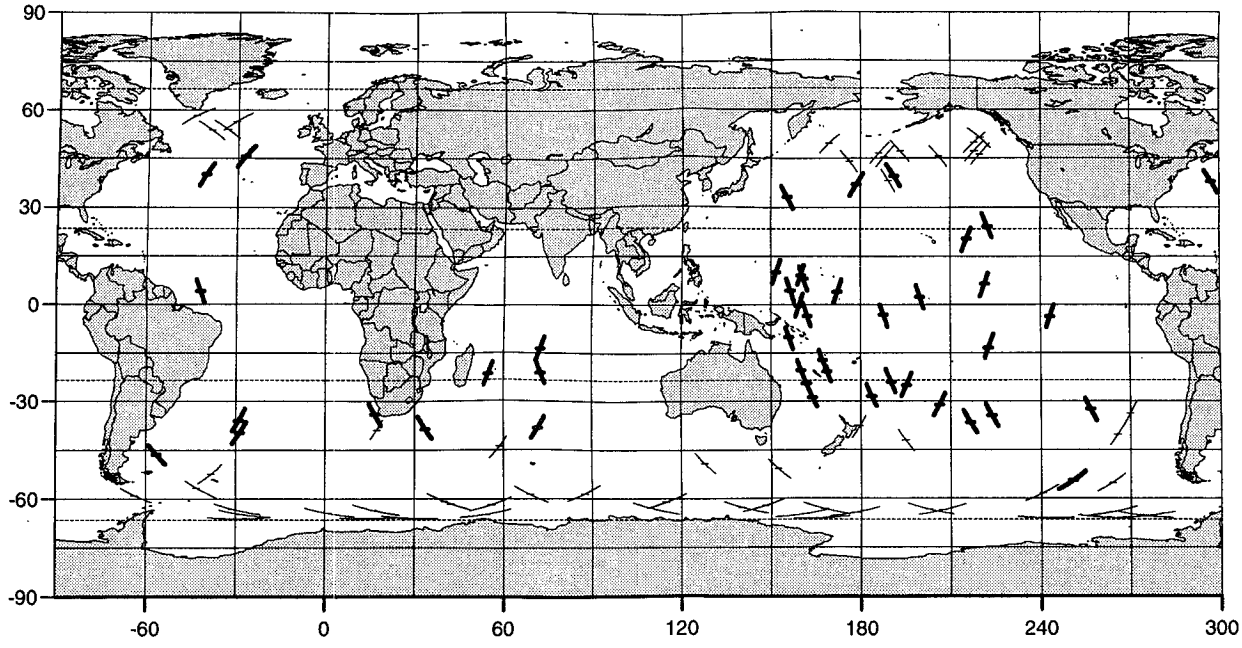

FIG. 11. Geographical plot of the location of sharp changes in K_u-band σ^0 values. [Criterion used is 2 dB or more change over nine records (~50 km) or less.] Plot is for the period 28 February–29 April 1993 (cycles 17–22), with the horizontal bars denoting the precise location of each event. Of the 101 cases, 44 contain points where T_b (37 GHz) exceeds 220 K; these are denoted by the thicker lines.

cipitation toward India and Southeast Asia, due to the southwest monsoon, corroborates the larger area of altimeter anomalies. Notice, too, that the size of the low precipitation areas in the subtropics shows the same seasonal behavior as the anomaly distribution described in the preceding paragraph.

Given that the altimeter and GPCC data are from different years and that monthly accumulations need not correlate well with what are essentially undersampled instantaneous rain attenuation events, the agreement is surprisingly good. More quantitative comparisons could be attempted by relating the monthly precipitation in each 2.5° × 2.5° box with the mean sigma0 anomalies from all altimeter data in the corresponding boxes for that month and year. Such activities are beyond the scope of the present study. However, it should also be noted that Figs. 12a and 12b relate to the frequency of occurrence of rainfall, whereas Figs. 13a and 13b are for mean rainfall rates. Using ships' *Present Weather* reports, Petty (1995) has looked at the fraction of rain observations that are classified as "drizzle" and noted that some regions have twice the proportion of their rain events being light than occurs in other areas.

The distribution of high liquid water events, as given by the TMR, has also been examined for March–April 1993. Occurrences in which LWP > 0.5 mm (not shown) look similar to the anomaly distribution. This is also true if the analysis is carried out in terms of points for which the rain flag is set, but then there are substantially fewer points. It appears that σ^0 deficits of 0.5 dB are comparable to LWP values of 0.5 mm (cf. section 5b and Fig. 10) and that a more stringent flagging procedure should be used if such effects are to be identified. These less severe events may correspond to thick nonprecipitating cloud rather than rain events, a hypothesis quite consistent with the theoretical values of Farrow (1975) for the attenuation coefficients.

A feature of the rain flag distribution is that it is rarely set at high latitudes. To explore this further, the 101 σ^0 jumps identified earlier have been reanalyzed using the 37-GHz brightness temperature, T_b (37 GHz), to distinguish between wind and rain-induced features. Using a threshold of 220 K indicated that 44 of the jumps were attributable to rain and that these were confined to ±45° latitude (Fig. 11). At high latitudes, the melting layer is generally much lower; this will tend to reduce both the microwave opacity of the rain layer and the pathlength for attenuation by liquid water. However, the temperature of the emitting layer of the atmosphere is also colder, possibly explaining the lower T_b values observed at higher-latitude events. Therefore, even the increased T_b of precipitating cloud may be below the 220-K threshold. Changing the threshold to 205 K increased the number of rain events to 52, while 190 K gave 60 such events, extending to about 60°. Most of the wind events are then confined to the Southern Ocean. Thus, there is a sensitivity to the T_b threshold value used, but it is not clear what latitudinal dependence should be used for identifying rain. A climatology of background values of T_b (i.e.,

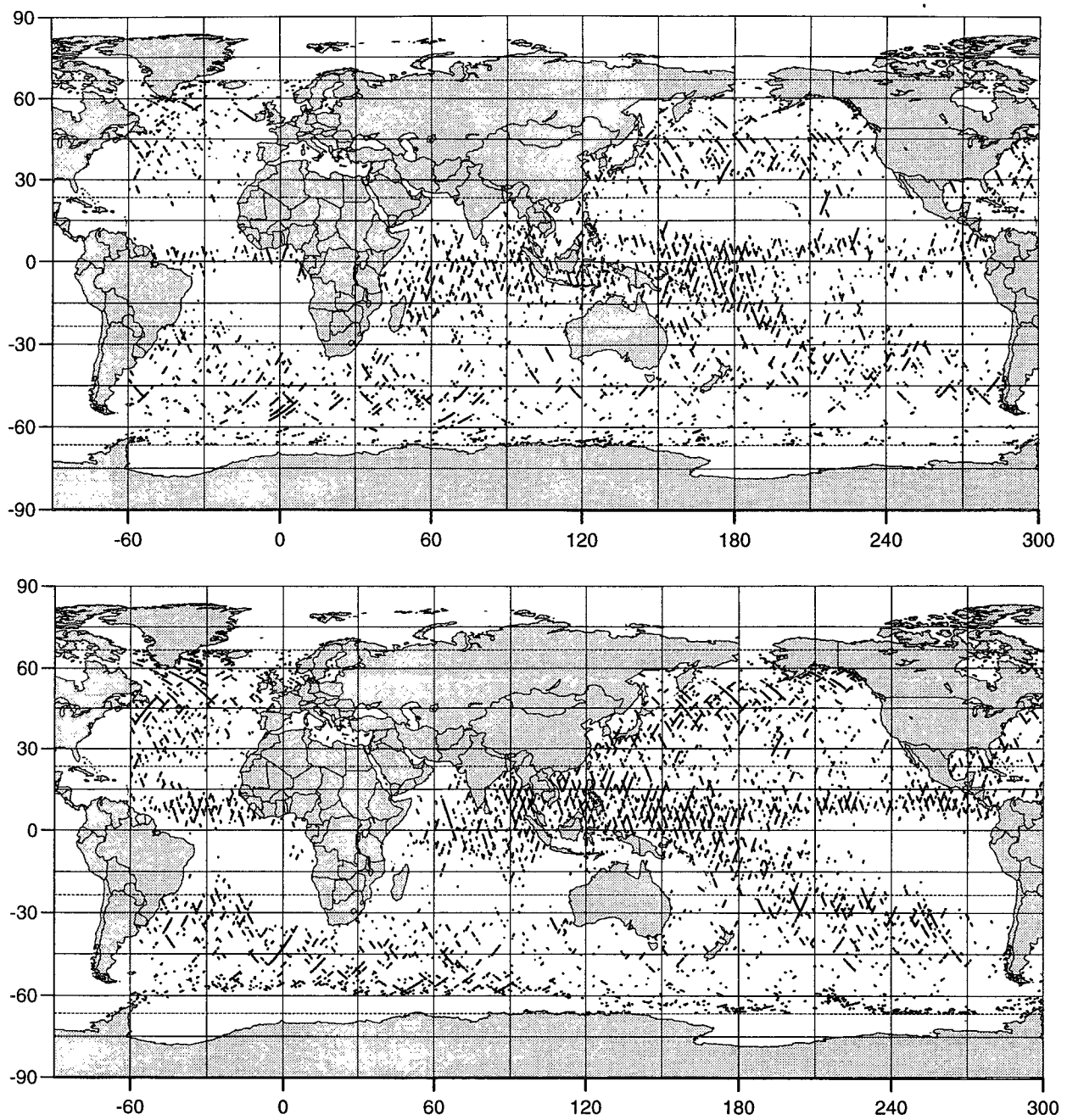

FIG. 12. (a) Geographical plot of all points during cycles 17–22 (28 February–29 April 1993) for which the sigma0 anomaly, $\Delta\sigma^0$, is less than −0.5 dB and the C-band σ^0 below 20 dB. (b) Same for cycles 35–40 (26 August–24 October 1993).

for noncloudy conditions) derived from passive microwave sensors would greatly assist in generating an appropriate rain flagging scheme.

c. *Location of altimeter inversions*

Lastly, we examine the distribution of inverted σ^0 behavior, that is, where K_u exceeds rescaled C band by at least 0.5 dB. It was thought that geographical patterns might be revealed, which would shed light on the mechanisms involved. (Note that this analysis precludes occasions in which both frequencies measure enhanced backscatter.) At first sight, the resulting distribution (Fig. 14) is generally similar to that of the K_u deficits during the same period (Fig. 12a), having zonal banding through the Tropics and midlatitudes and

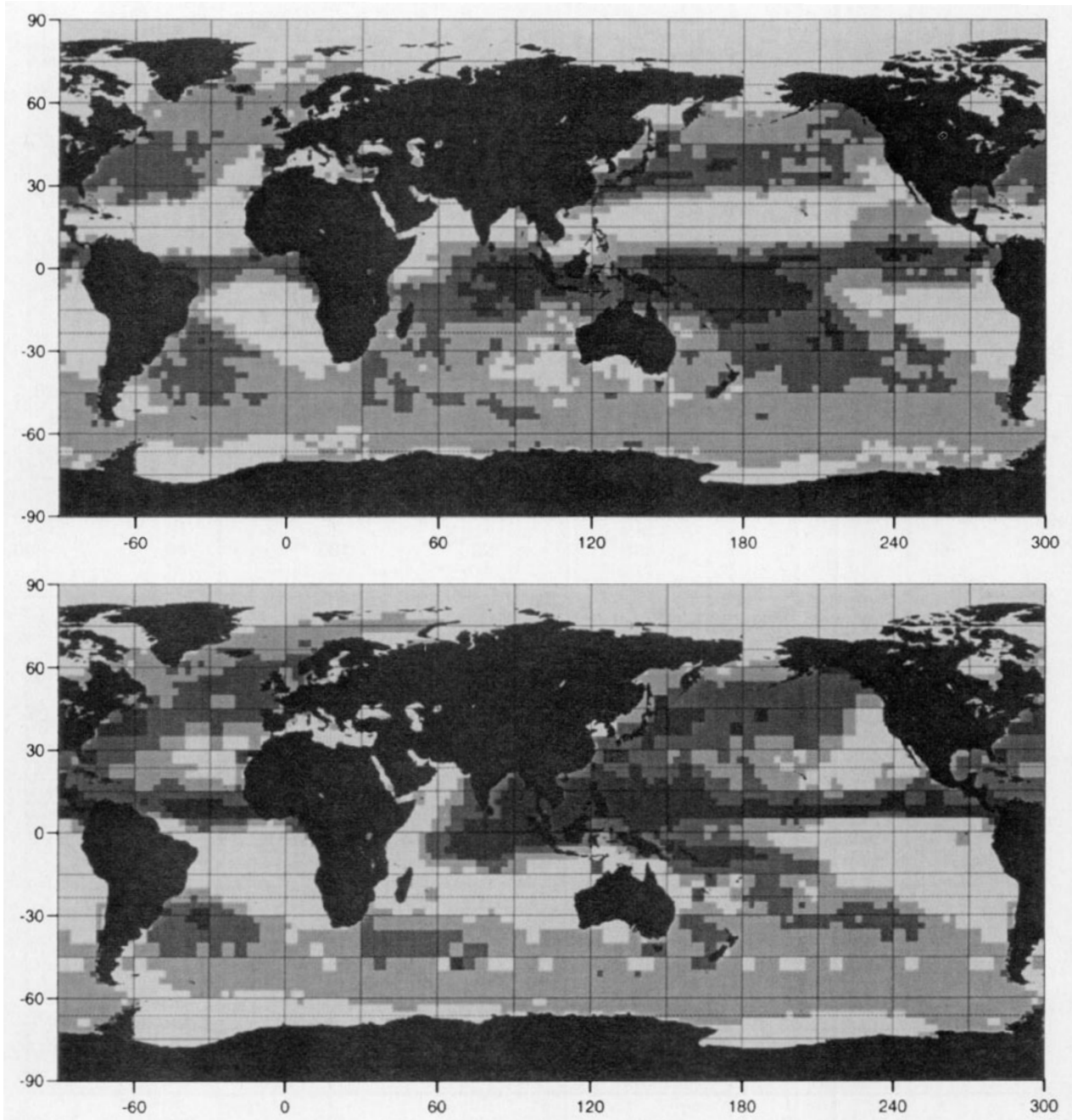

FIG. 13. Plot of global precipitation indices produced by the GPCC (1993), with light gray showing less than 50 mm month^{-1} and successively darker shades for 50–100, 100–200, and greater than 200 mm month^{-1}. Data are calculated from a combination of IR, SSM/I, land-based gauge data and ECMWF model output. (a) Mean monthly rainfall over March–April 1987 and 1988. (b) Same for September–October.

a marked absence of points in the subtropics. A major difference is that the number of times when $\Delta\sigma^0$ exceeds 0.5 is much smaller than the number of cases of $\Delta\sigma^0$ less than -0.5; this is particularly noticeable near the equator. Moreover, the length of track over which the inverted behavior is observed is shorter. This suggests that the inversions are associated with rain areas but that they do not require the intense precipitation of the Tropics. Reasons for K_u-band backscatter exceeding C band are not understood. One possibility is that extreme mispointing may have different effects at the two frequencies, but this has been discounted after a preliminary examination of the relationship between anomalies and indicated mispointing angle. Another

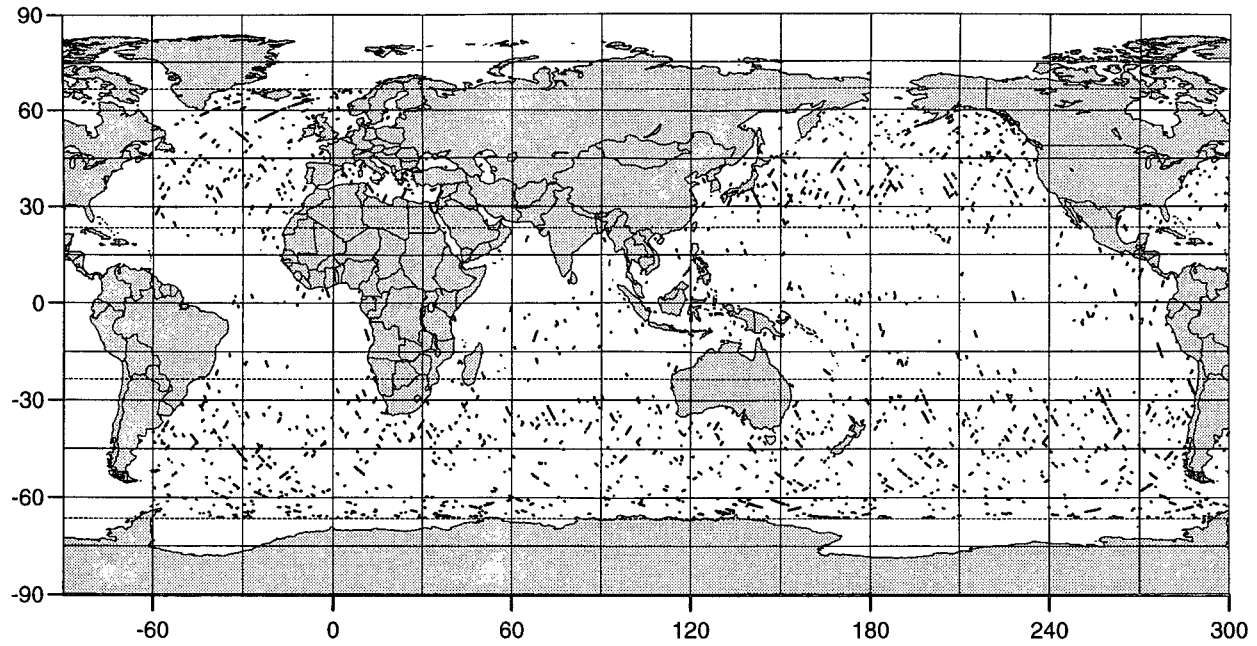

FIG. 14. Geographical plot of all points during cycles 17–22 (28 February–29 April 1993) for which the sigma0 anomaly, $\Delta\sigma^0$, is greater than 0.5 dB and the C-band σ^0 below 20 dB.

explanation is that an abrupt reduction in surface winds and the consequent loss of energy input to the short-wave field will allow the smallest waves (to which K_u is most sensitive) to dissipate more quickly than those at wavelengths to which C band responds. This topic requires further investigation. It should be noted that inversions need not be associated with cases of enhanced backscatter (section 4d); the latter may result in no significant difference between the rescaled σ^0 values. Conversely, inversions may occur without there being a significant peak relative to the general background.

7. Discussion and conclusions

While theoretical papers on the effect of rain on altimetry have been around for many years, there have been few published investigations using real data. Our earlier studies of K_u-band data from Seasat and *ERS-1* are summarized in section 1. In this paper, the serendipitous presence of a C-band radar on Topex is shown to have opened further avenues for investigation. The only other investigation, known to us, of the effects of rain on Topex data is a parallel investigation by Morland (1994).

Her investigation followed a similar approach to that used in this paper, including selection of rain events according to the criteria espoused by Guymer and Quartly (1993; see also GQS). However, the data used were from the first 10 cycles of the mission and cover only the North Atlantic. This precluded any investigation of geographical or temporal variations (such as occur for the ITCZ). Also, the preverification versions of data and algorithms were used in her analysis; this explains why she never finds the rain flag to be set. In keeping with our work, she associates deviations from a mean K_u–C σ^0 relationship with the presence of rain in the data. For sections across rain events, she used the observed attenuation dips in each of the frequencies to infer cloud heights and rain rates; however, the inversion amplifies the effect of measurement noise, yielding grossly unrealistic rain rates. Overall, where the studies overlap, Morland's (1994) results and those presented here are in agreement.

Theoretical analysis (Farrow 1975) has shown that the attenuation at C band should be much less than that at K_u band. However, to demonstrate this clearly, the power levels in the absence of attenuation need to be known. Since a thorough knowledge of radar interaction with the sea surface is still lacking, it was necessary to derive a simple empirical relationship between reflected power levels at K_u and C bands under conditions of minimal atmospheric moisture and use departures from this mean curve as a proxy for absolute attenuation.

Examination of a series of case studies confirmed expectations: after rescaling, C-band and K_u-band σ^0's agree well, except in localized regions, where the K_u values undergo a sharp decrease (often of several decibels, though of short duration), while C band shows only small changes, consistent with variation in the wind field. These sudden drops in K_u-band σ^0's are

attributed to attenuation by rain, an interpretation corroborated by the high brightness temperatures observed by the TMR. Several other geophysical variables derived from the altimeter return waveform—significant wave height H_s, standard deviation of height estimates σ_h, and attitude (not shown)—often show anomalous behavior on transit into a region of attenuation. This is entirely in keeping with the effect of localized intense rain on altimeter waveforms and their interpretation as geophysical variables as discussed in section 5 of GQS. [An examination of the Topex waveform product is left to a later paper (Quartly 1996, manuscript submitted to *J. Atmos. Oceanic Technol.*).] Although anomalous behavior in σ_h and sharp changes in range tend only to occur on entry and/or exit of a rain cell, there will be an error in the derived sea surface height field across a major storm due to commonly used parameterizations of the sea-state bias correction involving altimeter estimates of U_{10}, based on σ^0 (Gaspar et al. 1994). The case studies also illustrated two other effects: enhanced backscatter possibly due to damping of sea surface ripples by impinging rain drops (section 4d) and cases of inverse behavior, where the K_u-band σ^0's are larger than the rescaled C-band values over an appreciable distance along track (section 4f). The physical processes behind this latter effect are not as yet known. One possible explanation is that changes in the air–water temperature difference, for example, at an atmospheric front, may affect the wind friction velocity and hence the surface roughness in a way that differs at the scales at which K_u and C bands are sensitive.

In section 5 of this paper, rain observations by the altimeter were contrasted with those by the onboard microwave radiometer. The latter has a much broader footprint than the altimeter and is thus unable to resolve some of the sharp spatial variations. The radiometer readings also show saturation and thus cannot be used to distinguish between different levels of heavy rainfall, whereas attenuation measurements by an altimeter show no signs of saturation. However, there is as yet no true calibration for the attenuation experienced in the Topex altimeter data, although there are theoretical predictions relating attenuation to rainfall (e.g., Farrow 1975).

Because of the minimal attenuation experienced at C band, the rescaled C-band σ^0 values indicate the backscatter power that would be observed at K_u band in the absence of atmospheric liquid water. Wind algorithms, such as the modified Chelton–Wentz (Witter and Chelton 1991), applied to the rescaled C-band measurements should yield wind speed profiles more accurate than those from the K_u-band values. This could be important in studies of wind fields across major storms or in determining climatologies for areas where rain is prevalent.

It would be useful to be able to characterize the attenuation at K_u band in terms of various brightness temperatures so that data for Poseidon (which has no C-band altimeter) could be similarly corrected. However, while there is some correlation between various functions of brightness temperatures and Topex's sigma0 anomalies, the degree of scatter appears such that only a moderate improvement can be achieved.

As the discrepancies between K_u- and rescaled C-band σ^0's have been related to rain intensity, the altimeter adds further scope to studies of global oceanic precipitation. The altimeter's observation of a collection of instantaneous intense rain events shows the same geographical distribution as mean monthly precipitation levels derived from other instruments. The potential exists for synergistic studies of major storms using infrared images of cloud-top temperatures coupled with altimeter transects showing rainfall distribution integrated throughout the atmospheric column. Improvements in rainfall estimation over the oceans will increase the accuracy of determination of the freshwater budget, that is, precipitation minus evaporation, which plays an important part in the circulation of the ocean through its effect on the density of the surface water masses.

Acknowledgments. The altimeter GDRs used in this study were obtained from AVISO, whose assistance is gratefully acknowledged. The GPCC data came from the Global Precipitation Climatology Centre, Offenbach. Our thanks also to Phil Callahan of the Jet Propulsion Laboratory for help in unraveling various particulars of the Topex product.

REFERENCES

Apel, J., 1994: An improved model of the ocean surface wave vector spectrum and its effect on radar backscatter. *J. Geophys. Res.*, **99,** 16 269–16 291.

Atlas, D., 1994: Footprints of storms on the sea: A view from spaceborne synthetic aperture radar. *J. Geophys. Res.*, **99,** 7961–7969.

Barrick, D. E., 1974: Wind dependence of quasi-specular microwave sea scatter. *IEEE Trans. Antennas Propag.*, **AP-22,** 135–136.

Benada, R., 1993: *PO.DAAC Merged GDR (TOPEX/Poseidon) Users Handbook* (Version 1.0). Jet Propulsion Laboratory.

Brown, G. S., 1978: Backscattering from a Gaussian-distributed perfectly conducting rough surface. *IEEE Trans. Antennas Propag.*, **AP-26,** 472–482.

Callahan, P. S., 1993: *TOPEX GDR Users Handbook* (Draft-2). Jet Propulsion Laboratory.

——, D. W. Hancock, and G. S. Hayne, 1994a: A new sigma0 calibration for the TOPEX altimeter. *TOPEX/POSEIDON Res. News,* **3,** 28–32.

——, C. S. Morris, and S. V. Hsiao, 1994b: Comparison of TOPEX/POSEIDON σ^0 and significant wave height distributions to Geosat. *J. Geophys. Res.*, **99,** 25 015–25 024.

Chelton, D. B., E. J. Walsh, and J. L. MacArthur, 1989: Pulse compression and sea level tracking in satellite altimetry. *J. Atmos. Oceanic Technol.*, **6,** 407–438.

Eymard, L., A. Le Cornec, and L. Tabary, 1994: The ERS-1 microwave radiometer. *Int. J. Remote Sens.*, **15,** 845–857.

Farrow, J. B., 1975: The influence of the atmosphere on remote sensing measurements. Vol. 3: Microwave and radio wavelengths. Tech. Rep. HSDP-TP-7400-VOL-3; ESRO-CR (P)-355, Hawker Siddeley Dynamics Ltd., Hatfield, United Kingdom, 132 pp. [Available from FIZ Karlsruhe, Bibliographic Service, D-76344 Eggenstein-Leopoldshafen, Germany.]

Fedor, L. S., and G. S. Brown, 1982: Waveheight and wind speed measurements from the SEASAT radar altimeter. *J. Geophys. Res.*, **87,** 3254–3260.

Francis, R., and Coauthors, 1991: The ERS-1 spacecraft and its payload. *ESA Bull.*, **65,** 27–48.

Gaspar, P., F. Ogor, P.-Y. LeTraon, and O.-Z. Zanife, 1994: Estimating the sea state bias of the TOPEX and POSEIDON altimeters from crossover differences. *J. Geophys. Res.*, **99,** 24 981–24 994.

GPCC, 1993: Global area-mean monthly precipitation totals on a 2.5° grid for the year 1988 (Preliminary results, derived from rain-gauge measurements, satellite observations and numerical weather prediction results). Deutscher Wetterdienst Rep. No. DWD/WZN-1993/07-1, GPCC, Offenbach/Main, Germany, 20 pp.

Guymer, T. H., and G. D. Quartly, 1993: The effect of rain on ERS-1 altimeter data. *Proc. First ERS-1 Symp.: Space at the Service of our Environment,* Cannes, France, European Space Agency, 445–450.

——, ——, and M. A. Srokosz, 1995: The effects of rain on *ERS-1* radar altimeter data. *J. Atmos. Oceanic Technol.*, **12,** 1229–1247.

Jackson, F. C., W. T. Walton, D. E. Hines, B. A. Walter, and C. Y. Peng, 1992: Sea surface mean square slope from K_u-band backscatter data. *J. Geophys. Res.*, **97,** 11 411–11 427.

Klein, L. A., and C. T. Swift, 1977: An improved model for the dielectric constant of sea water at microwave frequencies. *IEEE Trans. Antennas Propag.*, **AP-25,** 104–111.

Marth, P. C., and Coauthors, 1993: Prelaunch performance of the NASA altimeter for the TOPEX/POSEIDON project. *IEEE Trans. Geosci. Remote Sens.*, **31,** 315–332.

Morland, J. C., 1994: The effect of rain on TOPEX/POSEIDON altimeter data. Tech. Rep. IFREMER No. 94-03, IFREMER, Brest, France, 84 pp.

Petty, G. W., 1995: Frequencies and characteristics of global oceanic precipitation from shipboard present-weather reports. *Bull. Amer. Meteor. Soc.*, **76,** 1593–1616.

——, and K. B. Katsaros, 1990: Precipitation observed over the South China Sea by the Nimbus-7 Scanning Multichannel Microwave Radiometer during winter MONEX. *J. Appl. Meteor.*, **29,** 273–287.

——, and ——, 1992: *Nimbus-7* SMMR precipitation observations calibrated against surface radar during TAMEX. *J. Appl. Meteor.*, **31,** 489–505.

Quartly, G. D., T. H. Guymer, and S. W. Laxon, 1994: Detection of rain cells in altimeter returns. *Proc. Second ERS-1 Symp.: Space at the Service of our Environment,* Hamburg, Germany, European Space Agency, 799–804.

Rodriguez, E., Y. Kim, and J. M. Martin, 1992: The effect of small wave modulation on the electromagnetic bias. *J. Geophys. Res.*, **97,** 2379–2389.

Srokosz, M. A., and T. H. Guymer, 1988: A study of the effect of rain on Seasat radar altimeter data. *Proc. IGARSS '88 Symp.*, Edinburgh, United Kingdom, European Space Agency, 651–654.

Stewart, R. H., 1985: *Methods of Satellite Oceanography.* University of California Press, 360 pp.

Tsimplis, M., and S. A. Thorpe, 1989: Wave damping by rain. *Nature,* **342,** 893–895.

Walsh, E. J., F. M. Monaldo, and J. Goldhirsh, 1984: Rain and cloud effects on a satellite dual-frequency radar altimeter system operating at 13.5 and 35 GHz. *IEEE Trans. Geosci. Remote Sens.*, **GE-22,** 615–622.

Wilheit, T. T., and A. T. C. Chang, 1980: An algorithm for retrieval of ocean surface and atmospheric parameters from the observations of the scanning multichannel microwave radiometer. *Radio. Sci.*, **15,** 525–544.

——, ——, M. S. V. Rao, E. B. Rodgers, and J. S. Theon, 1977: A satellite technique for quantitatively mapping rainfall rates over the oceans. *J. Appl. Meteor.*, **16,** 551–560.

Witter, D. L., and D. B. Chelton, 1991: A Geosat altimeter wind speed algorithm and a method for altimeter wind speed algorithm development. *J. Geophys. Res.*, **96,** 8853–8860.

Young, I. R., 1993: An estimate of the Geosat altimeter wind speed algorithm at high wind speeds. *J. Geophys. Res.*, **98,** 20 275–20 285.